Žune Ba-F epithermal deposit Part 1: mineralogical and geochemical characteristics

Borojević Šoštarić, Sibila; Roglić, Martin; Milošević, Aleksej; Brenko, Tomislav

Source / Izvornik: **Geologia Croatica, 2022, 75, 393 - 410**

Journal article, Published version
Rad u časopisu, Objavljena verzija rada (izdavačev PDF)

https://doi.org/10.4154/gc.2022.24

Permanent link / Trajna poveznica: https://urn.nsk.hr/urn:nbn:hr:169:169518

Geologia Croatica
Journal of the Croatian Geological Survey and the Croatian Geological Society
2022 | 75/3 | 393–410 | 14 Figs. | 1 Tab. | 2 Appendix Tabs. | www.geologia-croatica.hr

Žune Ba-F epithermal deposit Part 1: Mineralogical and geochemical characteristics

Sibila Borojević Šoštarić[1,*], Martin Roglić[1], Aleksej Milošević[2] and Tomislav Brenko[1]

[1] University of Zagreb, Faculty of Mining, Geology and Petroleum Engineering, Pierottijeva 6, HR-10000 Zagreb, Croatia; (*corresponding author: sibila.borojevic-sostaric@rgn.unizg.hr)
[2] Faculty of Mining, Bulevar vojvode Petra Bojovića 1A, 78000 Banja Luka, Republic of Srpska, Bosnia and Herzegovina

doi: 10.4154/gc.2022.24

Article history:

Manuscript received November 12, 2021
Revised manuscript accepted May 19, 2022
Available online October 26, 2022

Abstract

The Žune Ba-F epithermal deposit is situated in the Ljubija ore field (NW Bosnia and Herzegovina), within Upper Palaeozoic dolostone. A typical ESE-WNW Variscan vergency fault zone separates the dolostone from Lower Triassic schists and sandstones. External and internal pseudo-bedding, with massive, homogenous structure and partial limonitization characterizes the dolostone. Its geochemical composition exhibits low SiO_2 (1.33 – 2.06 mass. %), Al_2O_3 (0.27 – 0.38 mass. %), BaO (0.02 – 0.83 mass. %), ΣREE (5.7 – 9.4 ppm), Sr (61.7 – 120.4 ppm), Sm (0.3 – 2.2 ppm) and Eu (0.1 – 0.6 ppm), while having high CaO (30.24 – 32.38 mass. %), MgO (16.47 – 17.35 mass. %) and LOI (44.6 – 45.58 mass. %). The dolostone-mineralization contact zone consists of metasomatically recrystallised host dolostone with quartz and pyrite, where the presence of accessory tremolite, magnesiochloritoid and pyknite indicates peak formation conditions in the pre-mineralization phase with temperatures above 300°C. Two ore types are described: (i) Ba-F vein-type mineralization composed of barite – fluorite ± quartz, and (ii) hydrothermal breccia composed of coarse-grained fluorite and barite, surrounding fragments of dolostone, and occupying ≈20 % of the deposit. Mineralized samples show slightly elevated SiO_2 (2.20 – 5.53 mass. %) and Al_2O_3 (0.24 – 0.74 mass. %), low MgO (below 0.02 mass. %) and LOI (0.3 – 3.1 %), with high BaO (up to 50.74 mass. %), CaO (up to 66.03 mass. %), ΣREE (20 – 166 ppm), Sr (exceeding 1 mass. %), Sm (up to 118 ppm) and Eu (up to 44 ppm). Elevated Sr can be correlated to other barite epigenetic hydrothermal deposits in the Dinarides, interpreted as Ba-Sr substitution in the barite crystal lattice. Fluorite-rich samples are characterized by Y (0.6 – 49.2 ppm) and HREE enrichment, accompanied by depletion of LREE. The Ba-F deposit Žune, having variable REE concentration and a negative cerium and ytterbium anomaly corresponds geochemically to world-class fluorite deposits associated with carbonate sedimentary rocks.

Keywords: Ba-F mineralization, carbonate-hosted, Dinarides, mineralogy, geochemistry, structural geology

1. INTRODUCTION

Within the Central Dinarides, fluorite (CaF_2) or fluorspar, an important industrial mineral used in the metallurgical, ceramic and chemical industries, commonly occurs as a secondary mineral associated with the Upper Palaeozoic continental rift related deposits or younger post-collisional hydrothermal alteration. Examples of Upper Palaeozoic deposits are: (i) As-polymetallic deposits with fluorite (Hrmza, Mid-Bosnian Schists Mts.), (ii) carbonate hosted barite-fluorite deposits (Meovršje, Mid-Bosnian Schists Mts.; Žune, Sana-Una Palaeozoic) and (iii) carbonate-hosted barite-siderite-fluorite deposits (Vidrenja-Ljubija, Sana-Una Palaeozoic). An example of a younger occurrence is the Oligocene post-collisional pneumatolytic-hydrothermal alterations of the S-type granitoid (Motajica Mt.) (BOROJEVIĆ ŠOŠTARIĆ et al., 2022 and references therein). According to a new classification scheme (MAGOTRA et al. 2017), fluorite-bearing deposits in the Dinarides are divided into two types: (i) those associated with carbonate sedimentary rocks (Hrmza, Meovršje, Žune, Vidrenjak-Ljubija), have a variable REE concentration and low to moderate negative cerium and ytterbium anomaly and (ii) others associated with felsic igneous rocks (Motajica Mt.) having a strong positive yttrium and negative europium anomaly. Fluorite deposits associated with carbonate sedimentary rocks worldwide show low formation temperatures ranging between 100˚C - 150˚C and variable salinities between 12 wt% eq NaCl up to 22 wt% eq NaCl, implying epigenetic formation conditions, very similar to the Mississippi-valley type deposits (MVT) (BEJAOUI et al., 2013; RAJABZADEH, 2007; XU et al., 2012). However, at the Žune location, Sana-Una Palaeozoic, PALINKAŠ et al. (2016) reported ore-forming fluids of NaCl-$CaCl_2$-H_2O composition with highly variable salinity and a homogenization temperature between 100 - 310°C, implying epithermal conditions. Hydrothermal fluids were interpreted as being a mixture of high-temperature-high-salinity Permian evaporitic sea water, diluted by low-temperature-low-salinity marine or meteoric waters.

This study focused on the Žune Ba-F epithermal deposit situated in northwestern Bosnia and Herzegovina with the aims of (i) performing detailed field mapping and production of a local geological map of the Žune deposit; (ii) conducting a structural study of the Žune deposit, linking the major structures with certain geodynamic events; (iii) conducting a detailed sampling campaign of the mineralization and the host dolostone; (iv) conducting detailed mineralogical and geochemical studies; (v) conducting cluster hierarchical analysis using geochemical datasets (major, trace and REE elements) and (vi) contributing to the formation conditions and metallogenic understanding of this rare deposit type in the framework of the Dinarides orogeny. Furthermore, the manuscript discusses REE-Y patterns of barite-fluorite ore as fluorite is typically associated with several critical elements, including the REEs, Y, Nb and Zr with REEs frequently substituting for Ca in the fluorite structure (BAU & DULSKI, 1995; MAGOTRA et al., 2017).

2. GEOLOGY

2.1. Regional geological setting

Palaeozoic complexes in the Internal Dinarides are part of the Dinaridic Variscan basement and represent the southeastern continuation of the Palaeozoic complexes of the Eastern Alps. They are included in the nappe structures of the Internal Dinarides by south-westward directed thrusting and rest on the Adriatic carbonate platform units. The Dinaridic ophiolite zone is thrust onto Palaeozoic complexes and represents their northeastern boundary (PAMIĆ & JURKOVIĆ, 2002; Fig. 1). The Sana-Una Palaeozoic is a northwestern part of the Dinaridic Variscan basement units, which are palaeogeographically related to Apulia and Africa. The Sana-Una Palaeozoic mostly consists of Carboniferous flysch sequences (sensu KARAMATA et al., 1997), where MAJER (1964) determined low and very low–grade metamorphic conditions (quartz-feldspars-sericite-chlorite-mica-ankerite assemblage). Carboniferous flysch contains (GRUBIĆ et al., 2015; MILOŠEVIĆ et al., 2017): (i) a Lower-Middle Carboniferous pre-flysch (lower flysch) unit, with the alternation of deep-marine dark argillaceous schists and medium-grain sandstone; (ii) an olistostromatic unit with Devonian, Lower and Middle Carboniferous limestone (JURIĆ, 1971) clasts containing foraminifers, corals and cono-

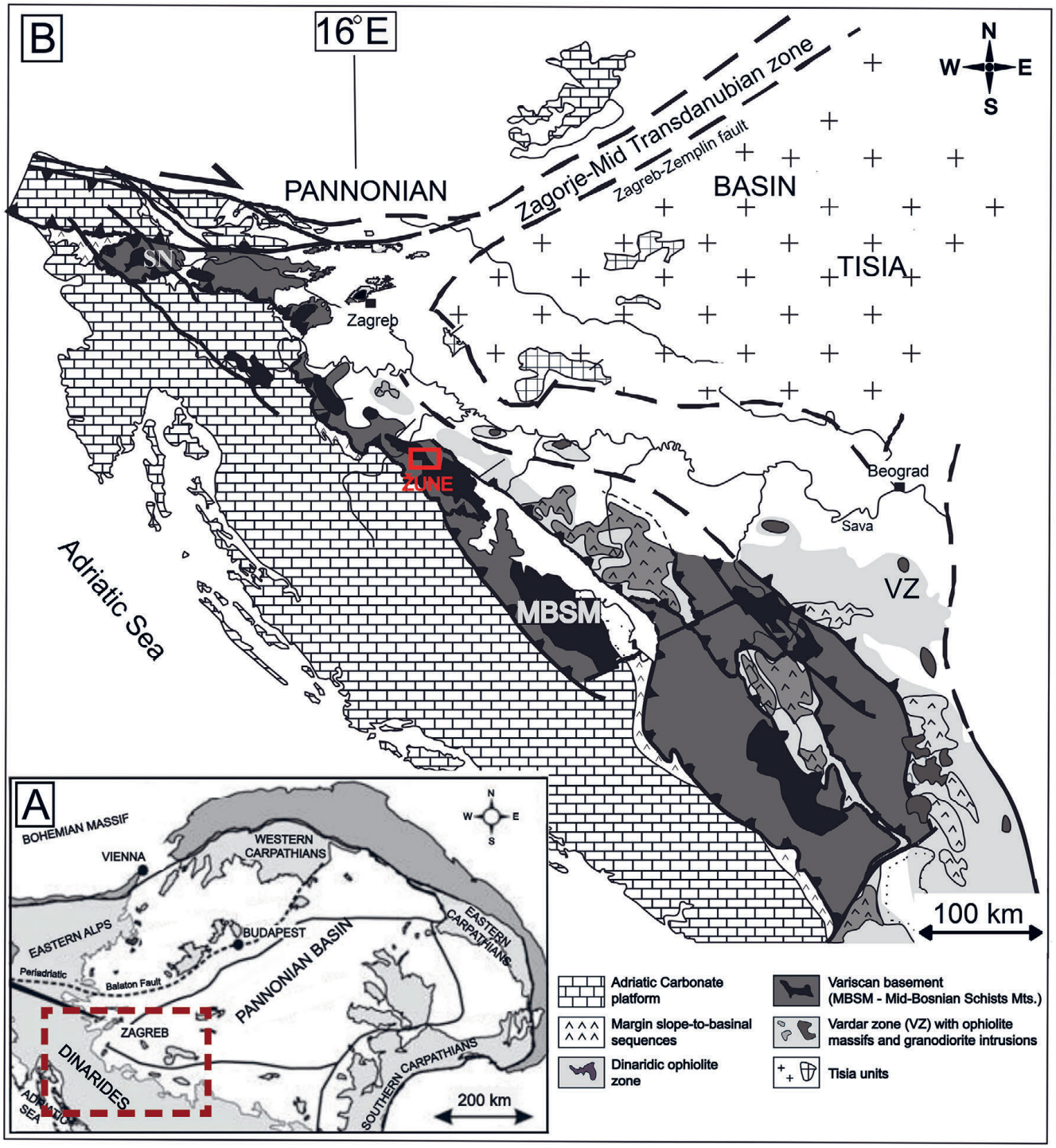

Figure 1. A) A simplified map of the Pannonian basin indicating the location of the Dinarides, B) A simplified geological map of the Dinarides with the major tectonostratigraphic units and the location of the Žune deposit (modified after PAMIĆ (1993), PAMIĆ et al. (1998), SCHMID et al. (1998), WILLINGSHOFER (2000) and TOMLJENOVIĆ (2002)).

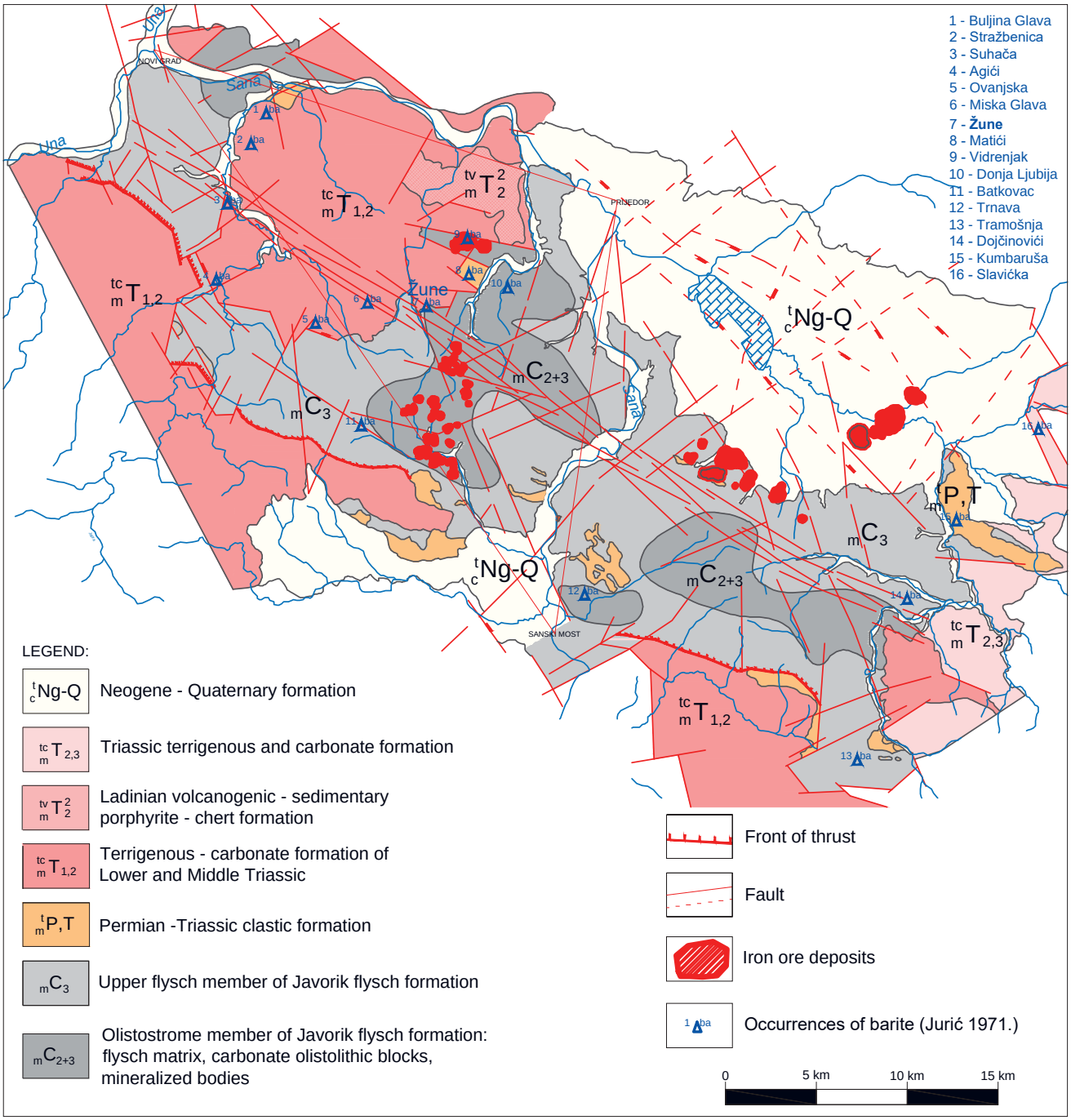

Figure 2. A tectono-geological map of the Sana-Una Palaeozoic (modified after GRUBIĆ et al., 2015).

donts, with this unit containing metasomatic mineralization represented by siderite and ankerite carbonates that serve as host-rocks for the largest iron deposit in the Dinarides, the Ljubija deposit, and (iii) the overlying Uppermost Carboniferous sandstone-siltstone flysch, black due to Mn-mineralization. Flysch sequences are overlain by Middle Permian clastic sediments (red breccia and conglomerates, sandstones, shales and evaporites) followed by Lower Triassic formations grading to limestone and dolostone and volcano-sedimentary chert formation (GRUBIĆ et al., 2000). Both Palaeozoic and Middle Permian to Triassic formations host numerous barite vein-type deposits (Fig. 2). All these formations are surrounded by Upper Jurassic and Cretaceous carbonates and Tertiary and Quaternary freshwater sediments that contain economically significant secondary iron ore deposits.

2.2. Local geological settings

The barite-fluorite vein-type deposit Žune, in the NW part of the Republic of Srpska region in Bosnia and Herzegovina, is located about 2.5 km from Ljubija town, at an altitude of 250 - 300 m above sea level and is surrounded by Kozara Mt. to the NE and the Majdanske Mts. to the SW. Host rocks are Upper Palaeozoic dolostones. Lower Triassic schists and sandstones located to the north and west of the mineralization are barren (Fig. 3). The structure and texture of the vein bears some elements of hydraulic fracturing, an important prerequisite for the boiling of hydrothermal fluid, as recognized in the fluid inclusion studies (PALINKAŠ et al., 2016). The barite-fluorite ore body is imprinted into porous dolostone along a fault zone with general strike ESE-WNW. This ore body is positioned subvertical with

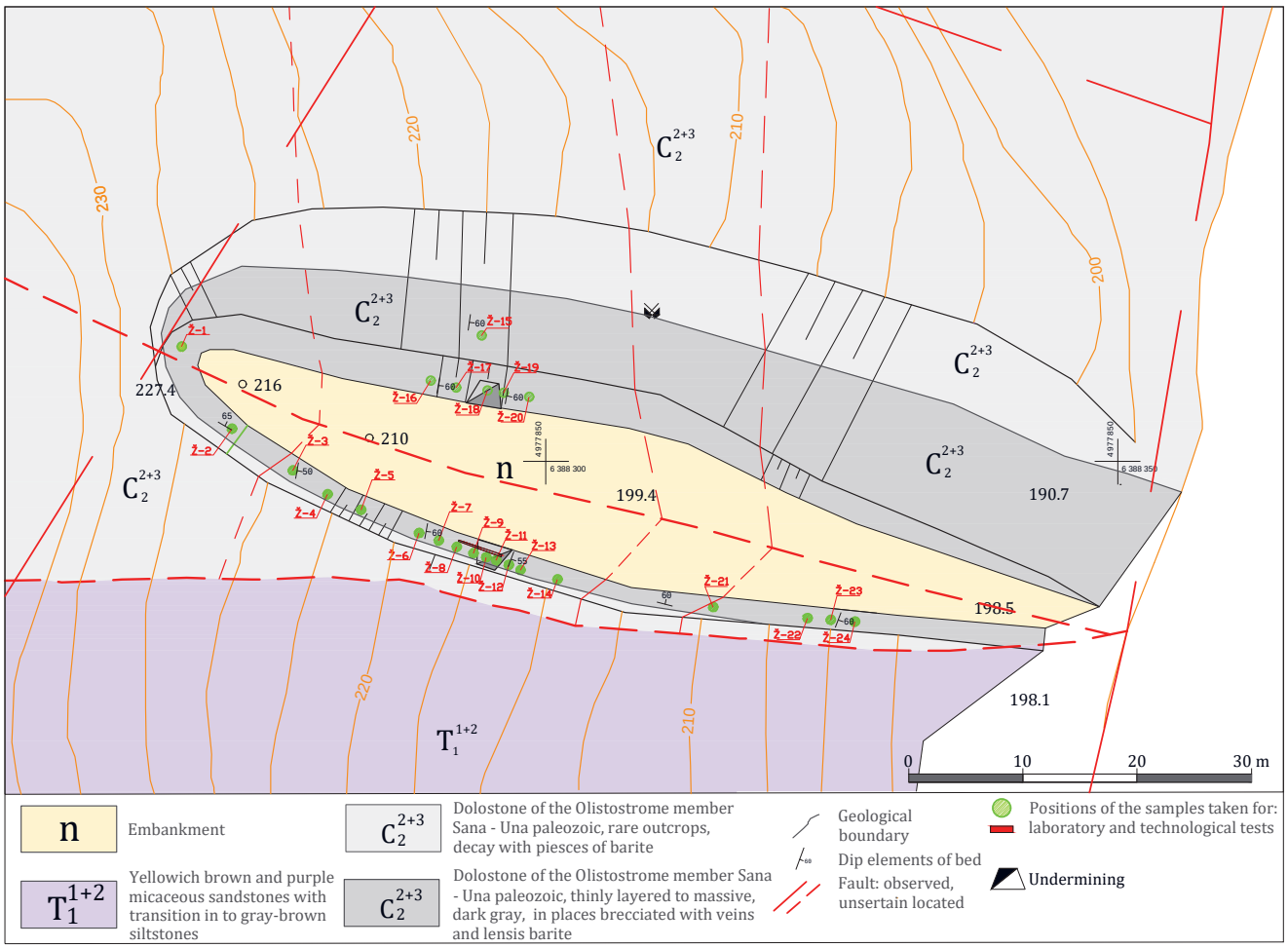

Figure 3. The local geological setting of the Žune deposit.

its thickness varying from 3 - 10 m, but in the higher levels can attain up to 20 m. The strike of the ore body can be followed for up to 50 m. The contact zone consists of metasomatically recrystallised host dolomite with strings of tiny barite veins and impregnations. Although alterations and metasomatic repression have been noticed, a sharp contact is common between the host rock and mineralised fault-related veins. The central part of the vein consists of pure barite and some fluorite. Barite occurs as white and massive in form in the SW part of the deposit whereas in the NE part it is mostly porous. Massive and porous barite is exposed on the surface in the middle part of the deposit. Fluorite also occurs in lenses or as impregnations within barite veins and dolostone, slightly postdating barite precipitation. Accessory minerals include calcite, quartz, sulphides and sulfosalts (tetrahedrite, cinnabarite, pyrite, realgar) and Au (JEREMIĆ, 1958). Quartz and fluorite occur in close contact, however, they do not contain solid inclusions. Pyrite is found on the contact with dolostone and as pyrite-quartz veinlets within the dolostone. Veinlets filled with calcite are rare and are also located in the contact zone. Pyrite is considered to have formed at the end of the pre-mineralization and beginning of the main mineralization phases, according to JEREMIĆ (1958). Sulfosalts (tetrahedrite and cinnabarite) observed by the previous author were formed during a post-mineralization phase, supressing the barite grains. The upper part of the ore body is limonitized.

The Žune barite-fluorite deposit, together with similar barite deposits in the Sana-Una Palaeozoic terrains was considered to be formed during the Permo-Triassic period by an early stage of intracontinental rifting of Tethys. The source of heat and hydrothermal fluids were deeply placed thermal diapirs (PALINKAŠ et al., 2016).

3. SAMPLES AND METHODS

Representative samples from the Žune epithermal Ba-F deposit were analysed micropetrographically using a LEICA MICROSYSTEMS 020-522 101 DM/LSP polarization microscope at the Faculty of Mining, Geology and Petroleum Engineering, University of Zagreb (n = 14; Table 1), and divided into three main groups (dolostone, Ba-F veins and hydrothermal breccia).

Geochemical whole-rock major and trace element analyses of the selected non-altered Žune samples (n=11; Appendix A) were conducted at the MSALabs Laboratory, Langley, Canada. Whole-rock major elements were analysed by inductively coupled plasma–atomic emission spectrometry (ICP–AES), while trace elements including rare earth elements were determined by inductively coupled plasma–mass spectrometry (ICP–MS). Lithium metaborate/tetraborate fusion and dilute nitric digestion were used for the decomposition of samples (0.2 g). Loss on ignition (LOI) was determined by weight difference after ignition at 1000°C. In addition, a separate 0.5 g split sample was digested in Aqua Regia and analysed by ICP-MS to determine the contents of precious and base metals.

Trace elements and REEs were analysed using the GCD Toolkit in R language (JANOUŠEK et al., 2006). Their contents

Table 1. List of samples with conducted analyses and mineral composition. List of mineral abbreviations: Brt = barite, Dol1 = host rock dolomite, Dol2 = contact zone recrystallized dolomite, Dol3 = late-stage fine-grained dolomite, Ep = epidote, Fl = fluorite, Lm* = limonite, Mcld = magnesiochloritoid, Py = pyrite, Tpz = topaz (pyknite), Tr = tremolite, Qtz = quartz.

Sample	Sample description	ICP-AES	ICP-MS	XRD	Micropetrography	Modal mineral composition	Accessory minerals	Alteration process
Ž-1	Dolostone	+	+		+	Dol1 (80%) > Qtz≈Brt≈Fl (5%) > Ms (1%)	Py	Lm, Dol2 (1%) > Dol3
Ž-2		+	+		+	Dol1 (85%) > Brt (5%) > Qtz≈Fl (3%) > Ms (1%)	Py	Dol2 (1%) > Lm, Dol3 (< 1%)
Ž-4		+	+		+	Dol1 (90%) > Fl (5%) > Qtz (3%)	Tr, Py	Lm (< 1%), Dol2
Ž-10		+	+		+	Dol1 (90%) > Fl (5%) > Qtz≈Ms (1%)	Py	Lm (< 1%), Dol2, Dol3
Ž-17		+	+		+	Dol1 (75%) > Fl (10%) > Qtz≈Brt (5%) > Ms (1%)	Tpz, Tr, Ep, Py	Lm (< 1%), Dol2, Dol3
Ž-3	Ba-F vein type mineralization	+	+		+	Brt (75%) > Fl (15%) > Dol1 (5%)	Py	Dol2 (3%) > Lm, Dol3 (< 1%)
Ž-11		+	+		+	Fl (95%) > Brt (3%) > Qtz≈Ms (1%)	Py	Lm (1%)
Ž-16		+	+	+	+	Fl (85%) > Brt (10%) > Qtz (3%) > Ms (< 1%)	Py	Lm (1%) > Dol2
Ž-19		+	+		+	Fl (90%) > Brt (5%) > Qtz≈Ms (1%)	Tr, Py, Tpz	Lm (1%) > Dol2
Ž-20		+	+	+	+	Brt (75%) > Fl (20%) > Ms (1%)	Py	Lm (1%) > Dol2
Ž-5	Hydrothermal breccia			+	+	Fl (50%) > Dol1 (20%) > Qtz (15%) > Brt (10%) > Ms (1%)	Mcld, Tr, Py, Tpz	Lm (1%) > Dol2, Dol3
Ž-6					+	Fl (80%) > Brt (10%); > Dol1 (5%) > Qtz (3%)> Ms (1%)	Py	Lm (1%) > Dol2
Ž-7		+	+	+	+	Brt (40%) > Qtz (35%) > Dol1 (15%) > Fl (5%) > Ms (1%)	Py	Lm (< 1%) > Dol2
Ž-22					+	Fl (55%) > Dol1 (35%) > Brt (5%) > Qtz (3%) > Ms (1%)	Py	Lm (< 1%), Dol2, Dol3

* - mineraloid

were normalized to chondrite (ANDERS & GREVESSE, 1989) and Upper Continental Crust (TAYLOR & MCLENNAN, 1995) and further plotted on the suitable diagrams.

The light fraction (quartz) was separated from the heavy fraction (barite) using sodium polytungstate – SPT in a centrifuge and then frozen while in cuvettes. Following this, the separation process was carried out by pouring deionized water over the frozen light fraction, thawing and separating it from the heavy fraction. The light fraction of each of the four samples was homogenized in an agate grinding set to powder fraction, and its mineral composition was determined using XRD analysis.

X-ray diffraction analysis of the selected samples was performed at the Faculty of Mining, Geology and Petroleum Engineering, University of Zagreb (n = 4; Table 1) following micropetrographical and geochemical analysis. A Malvern PanAnalytical vertical X–ray goniometer (type X'Pert MPD) was used, equipped with Cu tube and graphite crystal monochromator with the following experimental conditions: 45 kV, 40 mA, primary beam divergence automatic, irradiated length 0.5 mm, continuous scan (step 0.0131303º 2Q/s). Obtained spectra were analysed using X'Pert HighScore plus 2.1 PANalytical B.V. software.

In order to determine correlation of major elements with selected trace and REEs in the barite and fluorite zones, hierarchical clustering analysis (HCA) was conducted on samples Ž-3, 7, 11, 16, 19, 20 using a joint tree diagram. The dataset needed to be log-transformed as geochemical data does not follow a normal distribution. Standardization of the data followed after log-transformation to make sure that each variable was weighted equally. As a result of data standardization, new values Z (Z-value), with a mean of zero, were calculated and are measured in units of standard deviation. Hierarchical plotting of data was conducted using Statistica 12 (STATSOFT INC., 2012). As the main distance measure between the geochemical variables, the Euclidean distance was chosen for this study with Wards method as the linkage rule. The linkage process and grouping were repeated until all variables were connected, where the variables showing the largest similarity were grouped first.

4. RESULTS

4.1. Structural characteristics of the deposit

Geological mapping was conducted with the purpose of better understanding geological relationships in the study area. Mineralised fault-related veins and veinlets were the main structural elements that were investigated, alongside pseudo-bedding of the host dolostone that is related to millimetre thick intercalations of clay. The Žune deposit, like the microlocality itself, and its barite ore body is situated in a Variscan fault zone having ESE-WNW vergency. It is also important to mention a second, subparallel and barren fault, with a similar general strike that is situated 10-20 m south of the deposit, separating the olistostromatic unit of the Sana-Una Palaeozoic from Lower Triassic sediments. Additionally, there are several faults, perpendicular to the main ESE-WNW vergency fault zone, postdating the mineralization fault that crosscut the ore body in deposit with minor upturn.

Pseudo-bedding in the host dolostone is characterized by millimetre thick intercalations of clay. The thickness of the pseudo-bedding varies from 5 - 30 cm. Additionally, milli- to centimetre intervals within the dolostone occur in variable grey colours, steepening 50-55° toward the east and lying subparallel to the clay intercalations. On the northern and southern flanks of the main ESE-WNW vergency Ba-F vein, milli- to centimetre thick barite veinlets within the host dolostone, with maximum length of 0.5 metres, were observed:

(1) Veinlet system Sv_1 (statistical vein orientation 283/75) was registered parallel or approximately parallel to the pseudo-bedding of the host-dolostone (Fig. 4C). These veinlets are filled with barite and fluorite and appear in metre intervals for a couple of metres on the northern and southern flanks of the deposit.

(2) The Sv_2 system of barite-fluorite veinlets (Fig. 4B and 4D), having the highest importance regarding mineralization, with orientation 190/80, lie parallel to the main fault and its mineralization.

(3) Sv_3 veinlets/joints have a general orientation 105/55 and are occasionally filled with barite-fluorite mineralization (Fig. 4B and 4D).

(4) Additionally, Sv_4 and Sv_5 veinlet systems appear diagonal to the pseudo-bedding of the host-dolostone (Fig. 13B; Sv4 with orientation 53/50 and Sv5 with orientation 339/72) and are weakly distributed in the deposit. They are commonly filled with barite.

4.2. Host rock petrography

Macroscopically, dolostone has a massive, homogeneous structure and is mostly dark grey (Fig. 5A, Fig. 5C) but can also appear light grey in some samples (Fig. 5D). Despite primarily having a massive structure, three samples (Ž-5, Ž-6, Ž-7; Figs. 8A

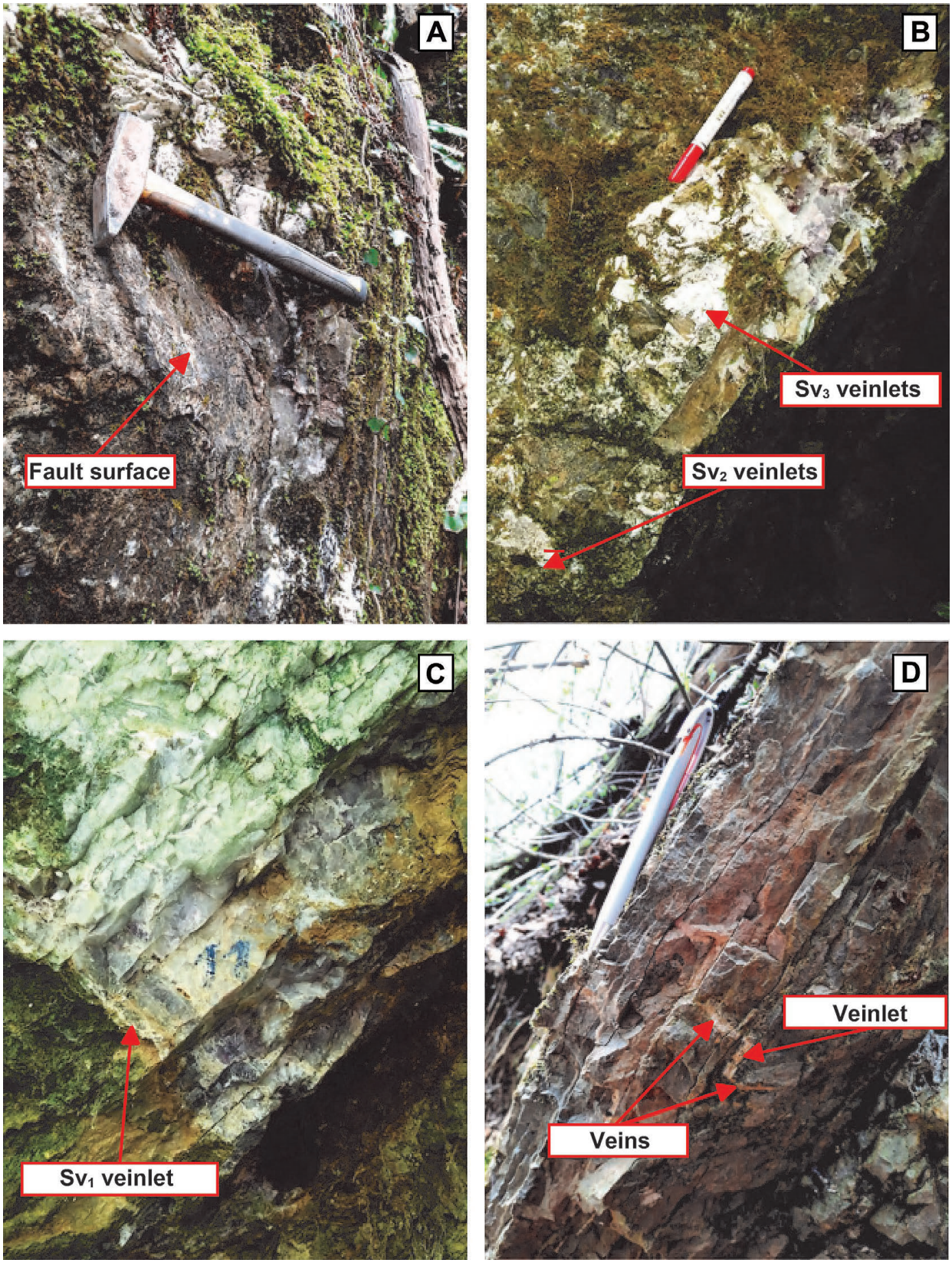

Figure 4. Structural elements in the Žune Ba-F deposit. A) Fault surface with ESE-WNW strike, eastern side of the canyon (Ž-22 sampling locality); B) Barite-fluorite vein within dolostone (Ž-21 sampling locality); C) cross tension Sv_1 vein in Ž-11 sampling locality; D) transition from pseudobedding to cross veins/veinlets in Ž-2 sampling locality.

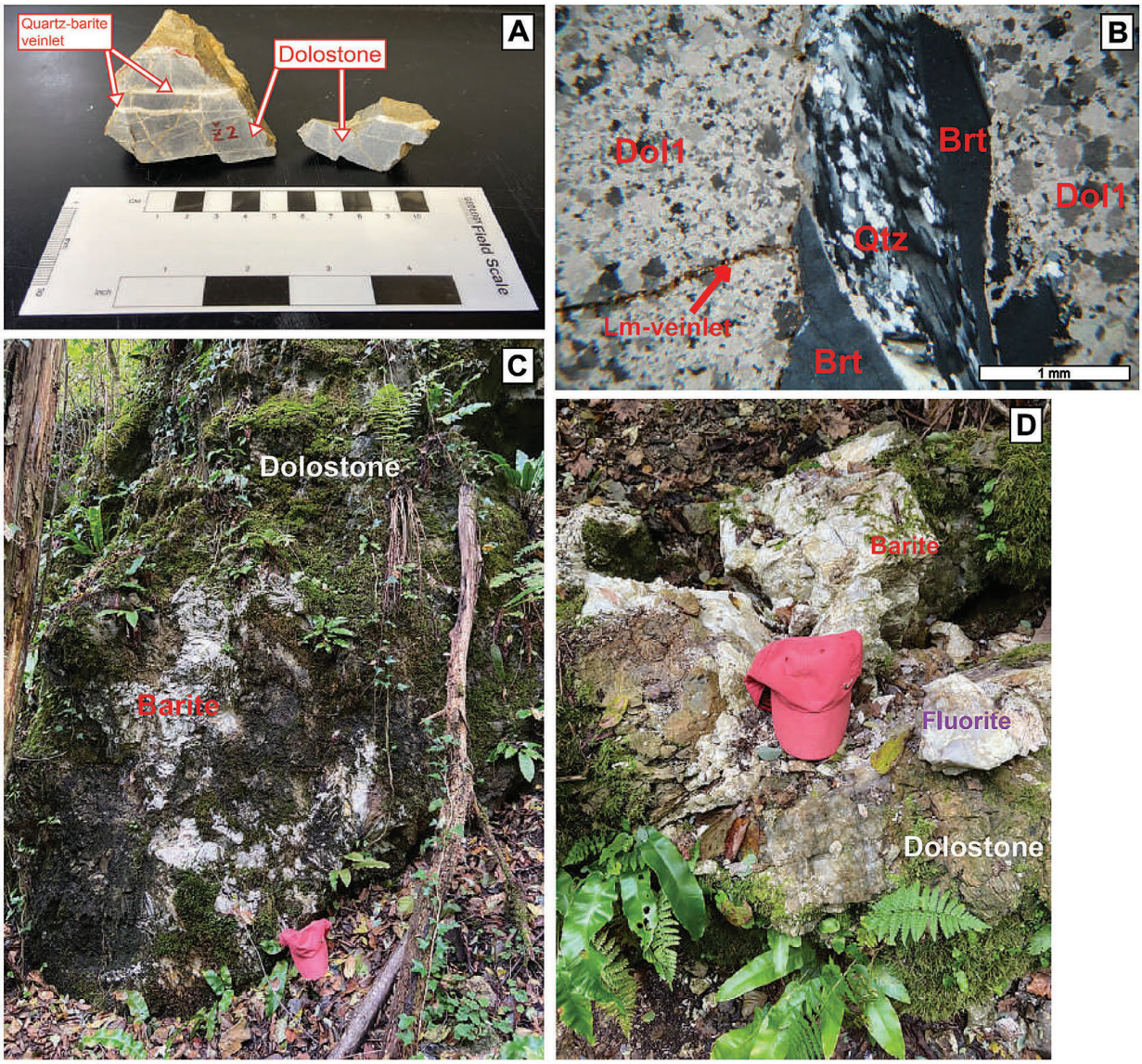

Figure 5. A) Quartz-barite veinlets cutting dolostone sample Ž-2, dark grey in colour; B) A photomicrograph of the Ž-2 sample (N+). Quartz-barite veinlet cutting dolostone (Dol1) which consisted of partly weathered dolomite mineral grains; C) Dolostone-barite outcrop on the left slope in the Žune deposit; D) Fluorite-barite-dolostone outcrop in the Žune deposit.

and 8B) of dolostone fragments are found as part of a breccia alongside barite and fluorite. Limonitization, occurring due to the alteration of sporadic pyrite grains, is present in the form of orange to brownish layers, and completely affects samples Ž-3 (Fig. 7A) and Ž-9 (Fig. 7B). In the proximity of the ore mineralization, veinlets are more common, occupying up to 15 vol. % of the dolostone. The thickness of veinlets ranges from 1.00 - 5.75 mm.

The micropetrographical study illustrates the presence of anhedral to subhedral mineral grains of dolomite (Fig. 5B). Dolostone is composed of dolomite mineral grains with negligible amounts of muscovite and opaque pyrite. The size of dolomite mineral grains varies from 0.008 - 1.20 mm, whereas the size of muscovite mineral grains varies from 0.004 - 0.18 mm.

4.3. Contact zone petrography

The contact zone between the Ba-F type of mineralization and dolostone is characterized by hydrothermally recrystallised dolomite (Dol2), pyrite and quartz containing accessory tremolite, magnesiochloritoid, topaz (pyknite), epidote and rutile. Small amounts of early-stage fluorite and barite are also present. Fine-grained late-stage dolomite veinlets (Dol3) sometimes crosscut all the earlier paragenesis (Fig. 6A). Limonitization after pyrite is widespread. Hydrothermally recrystallised dolomite (Dol2) and quartz are coarser-grained (from 0.2 - 1 mm in size), compared to euhedral pyrite that occurs as fine grains (0.01 - 0.25 mm). Accessory minerals are similar in size to the pyrite. Tremolite (1 vol. % of the thin sections) mostly occurs as a fibrous aggregate on the contact between quartz and early-stage fluorite but can also be found incorporated in both quartz and early-fluorite grains (Fig. 6B). Radially shaped aggregates of magnesiochloritoid (2 vol. % of the thin sections) occur included within quartz grains (Fig. 6B). Acicular mineral grains of pyknite ($[Al_2(SiO_4)(F,OH)_2]$; 1 vol. % of the thin sections) are commonly included within quartz (Fig. 6D). Dimensions of the pyknite mineral grains vary from 0.003 - 0.17 mm. Epidote (1 vol. % of the thin sections) is present as granular aggregates or as individual mineral grains (Fig. 6C) sometimes included in quartz. Dimensions of epidote mineral grains vary from 0.02 - 0.16 mm. Early-stage barite is tabular to coarse-grained, does not host solid inclusions and appears similar to barite in vein and breccia types of mineralization.

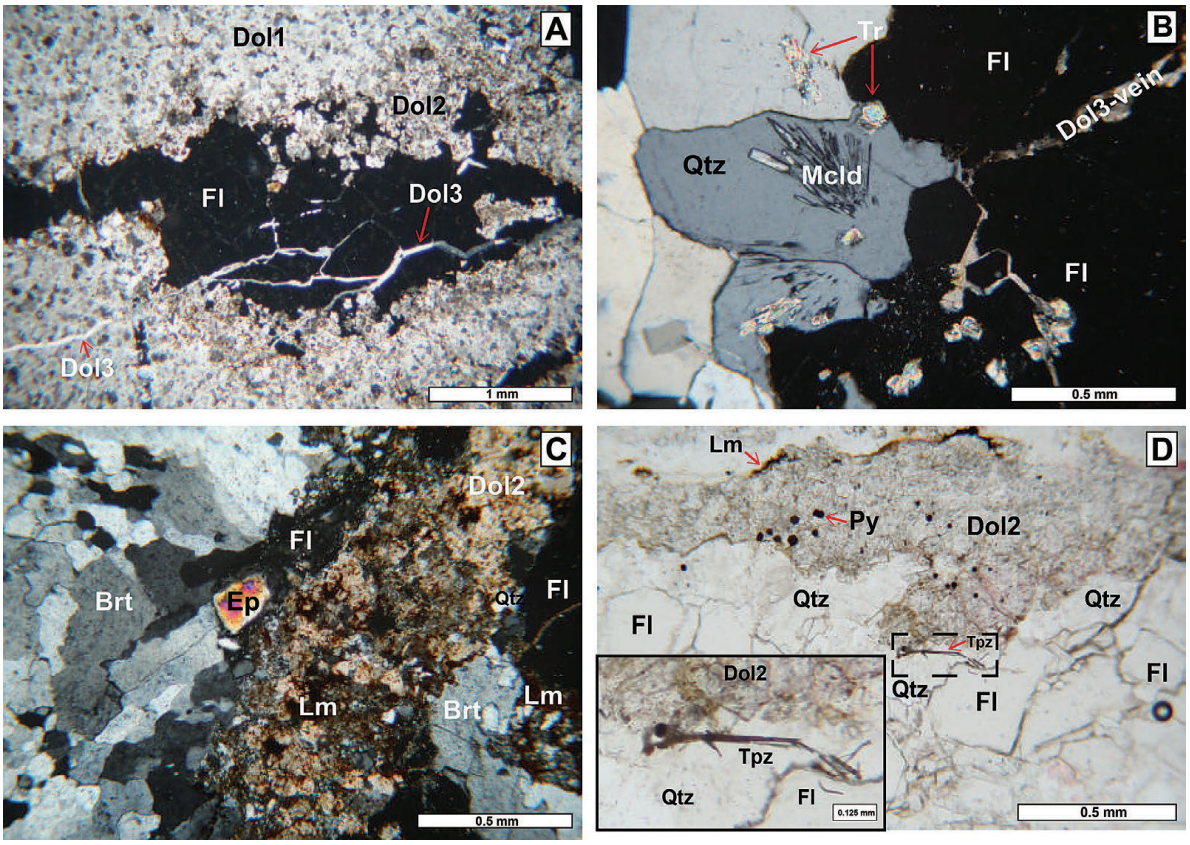

Figure 6. A) A photomicrograph of the Ž-1 sample (N+). Host dolostone (Dol1) in contact with recrystallised dolomite (Dol2) and a barite/fluorite vein cross-cut by fine-grained late-stage dolomite veins (Dol3); B) A photomicrograph of the Ž-5 sample (N+). Radially shaped magnesiochloritoid and tremolite included in quartz surrounded with fluorite that is cross-cut by late-stage dolomite (Dol3); C) A photomicrograph of the Ž-9 sample (N+). Epidote grain in contact with fluorite and limonitized dolomite; D) A photomicrograph of the Ž-17 sample. Topaz (pyknite) included in quartz on border with recrystallised dolomite. Euhedral pyrite present inside dolomite. Brt = barite, Cb = carbonate mineral, Dol1 = host dolostone, Dol2 = recrystallised dolomite, Dol3 = late-stage dolomite, Ep = epidote, Fl = fluorite, Lm = limonite, Mcld = magnesiochloritoid, Py = pyrite, Tpz = topaz (pyknite), Tr = tremolite, Qtz = quartz.

4.4. Ore petrography

4.4.1. Ba-F vein type of mineralization

The predominant type of mineralization in the Žune deposit is the Ba-F vein type mineralization located within a fault zone with a general strike of ESE-WNW. The main Ba-F vein is subvertical, 3 - 10 m thick and up to 50 m in length and composed predominantly of barite and up to 20% fluorite. The mining operations stopped in the late 1950s due to an increasing amount of fluorite with depth (JEREMIĆ, 1958). Quartz and hydrothermal carbonates occur as accessory minerals. Smaller veinlets (<1 - 6 mm thick) of similar composition occur within the dolostone (Figs. 7A, 7B). Fluorite and quartz are usually located on the veinlet's edges indicating slightly earlier deposition. In the central part of the veinlets, barite is the dominant phase while fluorite, quartz and other minerals are less abundant.

The micropetrographical study illustrates the presence of fluorite and barite as the main ore minerals alongside quartz in the examined samples. Fluorite is mostly coarse-grained, isotropic with expressed cleavage. Dimensions of fluorite grains vary from 0.05 up to 5.50 mm. Fluorite occupies 15–95 vol. % of thin sections. Barite occurs as fine-grained to coarse-grained, elongated or as fan-shaped aggregates. Dimensions of barite grains range from 0.1 to 4.50 mm, occupying 3–85 vol. % of thin sections. Quartz occurs in smaller amounts in thin sections (1–3 vol. %) with grain size varying between 0.02 - 3.50 mm. Quartz is often found accompanied by fluorite in veinlets, and seldom by barite.

4.4.2. Hydrothermal breccia

The hydrothermal breccia mostly occurs in proximity to the contact zone, represented by the Ž-5, Ž-6, Ž-7 and Ž-22 samples. Fluorite-barite-dolostone-quartz breccia makes ≈20 % of the deposit. The Ž-6 (Fig. 8A), Ž-7 and Ž-22 samples predominantly consist of fluorite and barite cement surrounding sporadic dolostone fragments with rare limonite veinlets, where fluorite and barite together comprise 60 vol. % of these three breccia samples. The Ž-5 sample (Fig. 8B) consists mostly of dolostone with quartz-limonite veinlets, where fluorite and barite occupy a minor part of the sample. Fluorite and barite together comprise 20 vol. % of the Ž-5 sample. Fluorite colour varies from purple to colourless with vitreous lustre. Barite is white in colour with a pearly lustre. Dolostone is dark grey in colour and partly limonitized. Barite, fluorite and quartz have similar physical and optical properties as those in Ba-F vein type mineralization samples.

4.5. Depositional succession

A simplified paragenetic sequence of minerals in the Žune deposit is presented in Figure 9. Based on microscopic analysis, it was determined that after recrystallised dolomite was formed in the pre-mineralization phase (Dol2), pyrite is the first to crystallize followed by minor quartz hosting accessory epidote, Mg-chloritoid, topaz (pyknite), tremolite and rutile and small amounts of early fluorite and barite. The main mineralization phase starts with abundant barite, fluorite and some quartz hosting accessory minerals. Small amounts of late-stage dolomite (Dol3) postdate previous phases (Fig 6). Limonite occurs in the post-mineralization phase as an alteration product of pyrite.

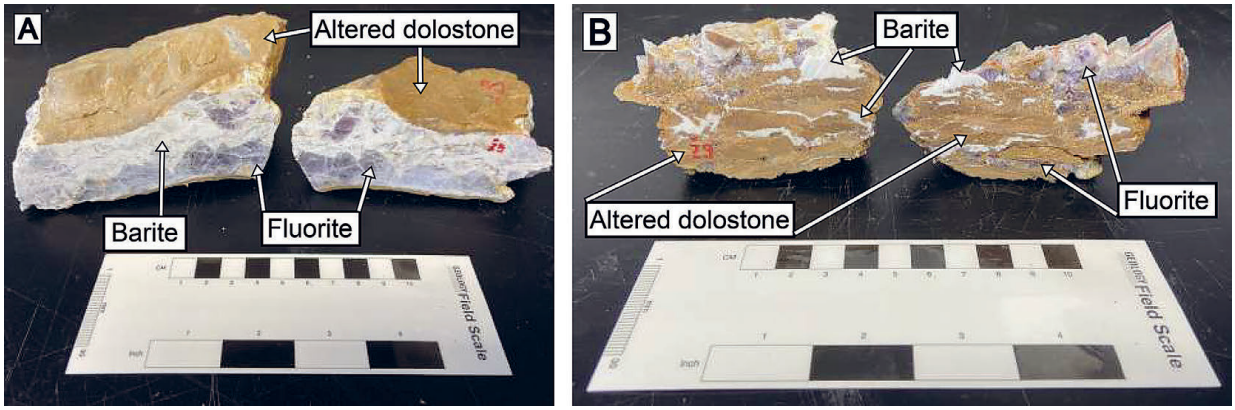

Figure 7. A) Barite-fluorite vein within limonitized dolostone present in shape of thin layer on the edges of Ž-3 sample ; B) Light to dark purple fluorite and white coloured barite occur in completely limonitized dolostone in Ž-9 sample.

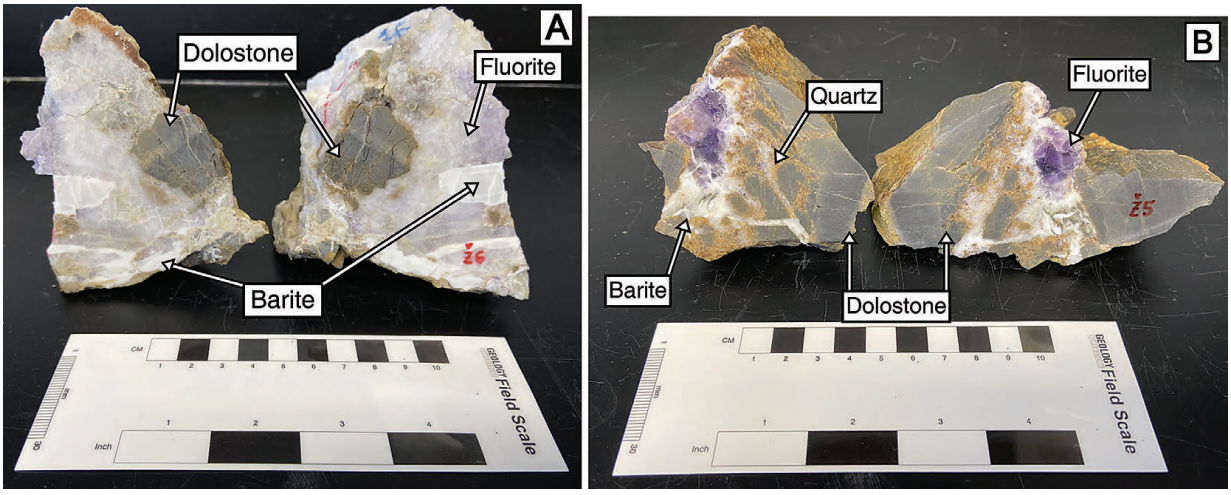

Figure 8. A) Ž-6 sample consisting of light purple to colourless fluorite, white barite with pearly lustre and dark grey dolostone in the form of breccia; B) Ž-5 sample present in the form of breccia with dolostone as a dominant component alongside deep purple fluorite, barite and quartz.

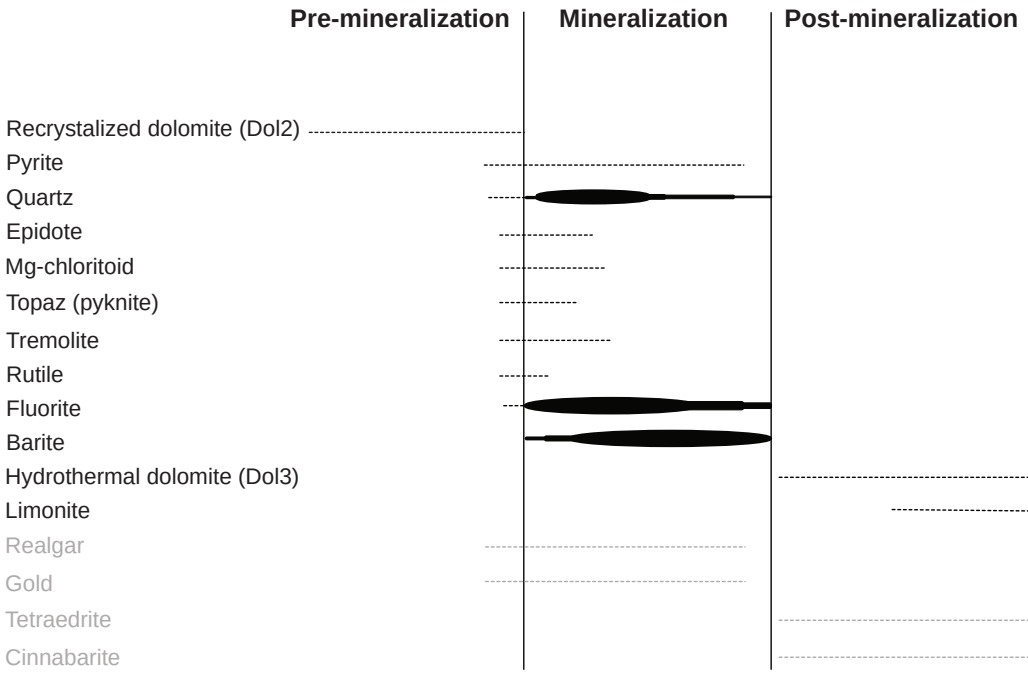

Figure 9. A simplified paragenetic sequence of minerals in the Žune deposit determined in this study. Minerals in light grey determined in previous study by JEREMIĆ (1958).

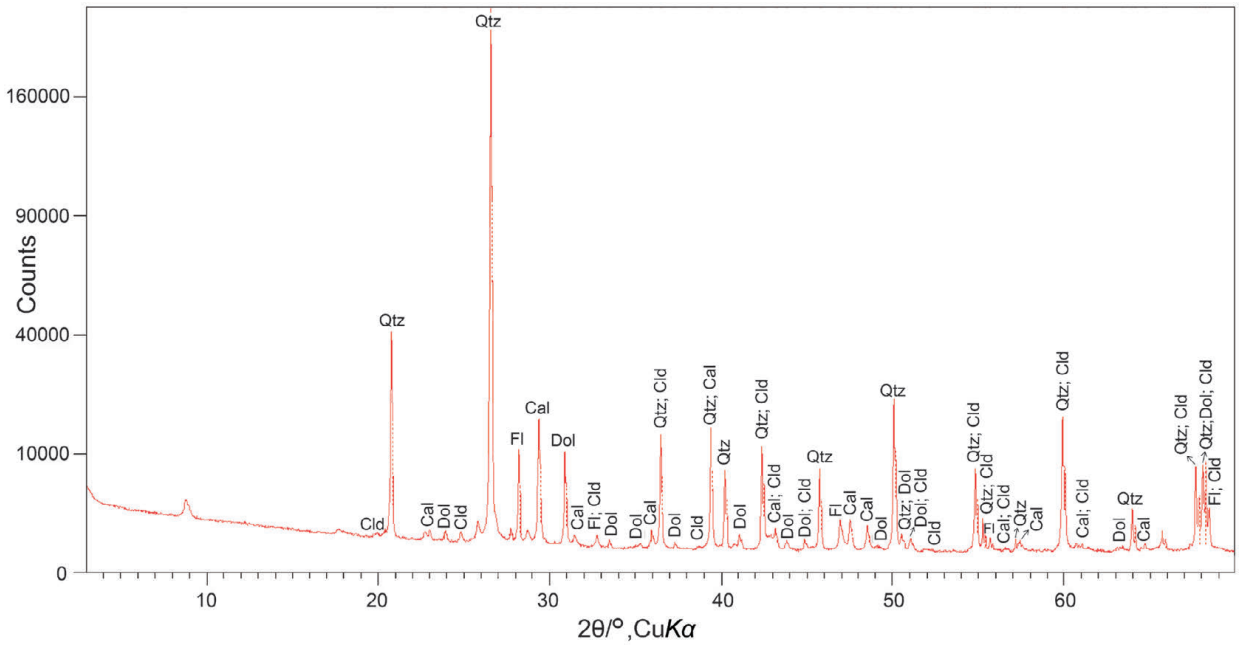

Figure 10. Results of XRD analysis for Ž-5 sample (Dol = dolomite, Cal = calcite, Fl = fluorite, Qtz = quartz, Cld = chloritoid).

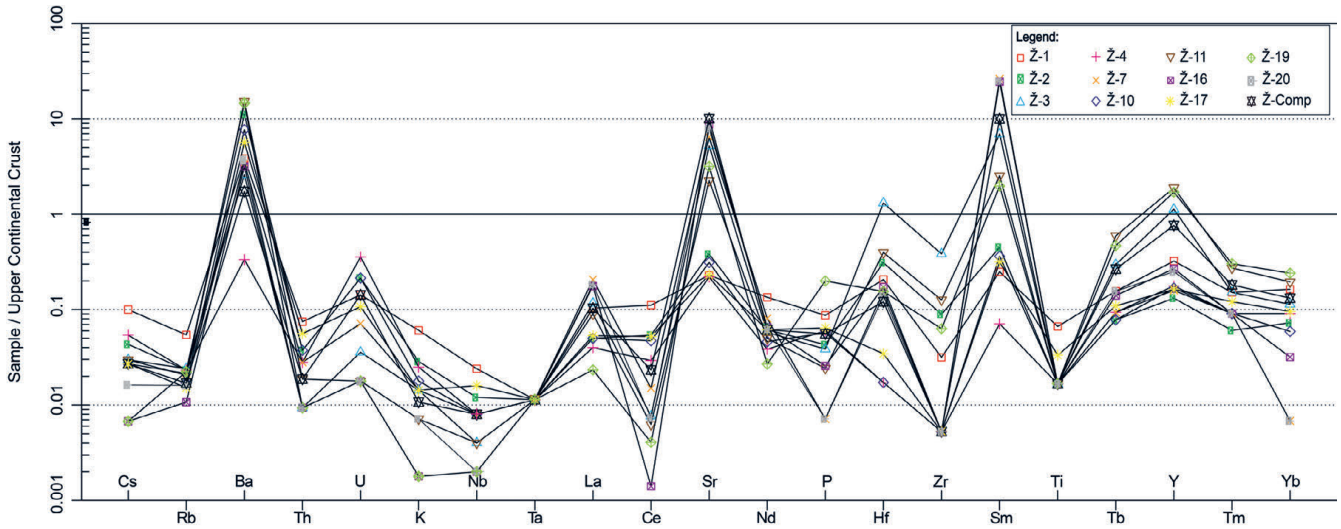

Figure 11. Trace element concentrations of samples Ž-1, Ž-2, Ž-3, Ž-4, Ž-7, Ž-10, Ž-11, Ž-16, Ž-17, Ž-19 and Ž-20 with Ž-Comp (= Ž-Composite) normalized to Upper Continental Crust (TAYLOR & MCLENNAN, 1995).

4.6. XRD analysis of the light mineral fraction

Based on the XRD analysis of the Ž-5 light mineral fraction, the most dominant mineral phases are dolomite, calcite and fluorite. Occasionally, quartz and chloritoid mineral phases are also observed (Fig. 10). Peaks of mineral phases, observed in thin-section (muscovite, barite, tremolite, pyknite, pyrite and limonite) were not recognized on diffractograms due to their low quantities in the Ž-5 sample. Samples Ž-7, Ž-16 and Ž-20 have a similar mineral paragenesis consisting of fluorite and quartz, with the occasional occurrence of dolomite.

4.7. Geochemistry

4.7.1. Major elements

The geochemical composition of the major elements is presented in Appendix A. Dolostone samples mostly consist of CaO (30.24 – 32.38 mass. %), MgO (15.62 – 17.35 mass. %) and loss on ignition (LOI) (43.61 – 48.58 mass. %). Only SiO_2 (1.33 – 3.65 mass. %) and F (2.55 – 3.16 mass. %) are present in significant contents, while other major elements are present in trace amounts. In contrast, samples of Ba-F vein-type mineralization have more variable geochemical composition. Two main components are CaO (6.3 up to 66.03 mass. %) and BaO (3.92 up to 50.23 mass. %). A positive correlation can be seen between BaO and SO_3 contents (2.05 up to 26.22 mass. %) and between CaO and CaF_2 (2.01 up to 22.88 mass. %). Only SiO_2 with values between 2.92 and 5.77 mass. % and LOI (0.3 up to 3.12 mass. %) are present in significant values, while other major elements are present in trace amounts.

4.7.2. Trace elements

The distribution of trace elements is similar in most of the analysed samples. It is also evident that the samples show trace element concentrations (Appendix A) mostly lower than the average

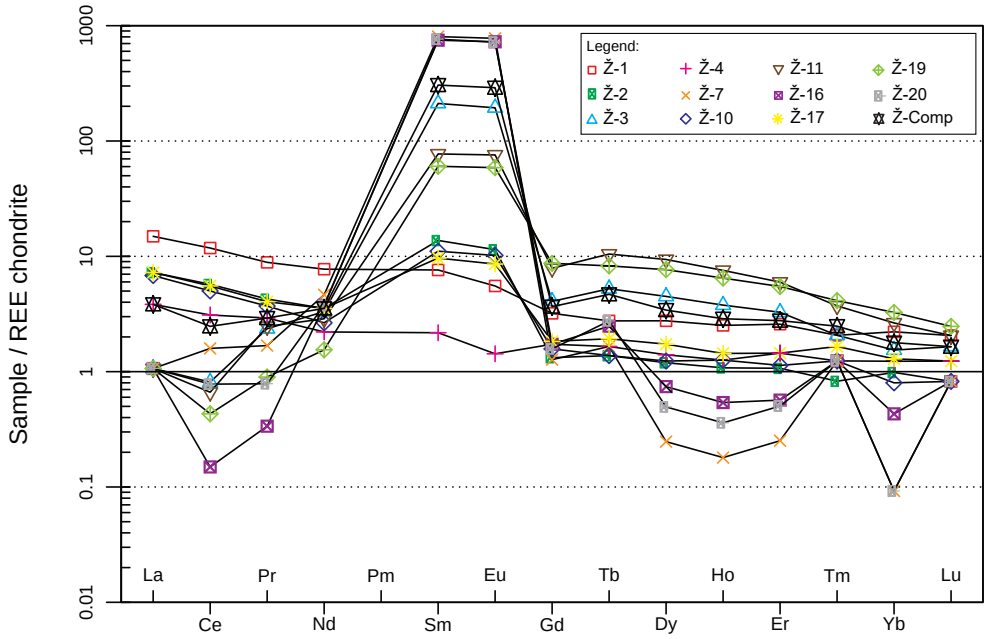

Figure 12. The chondrite normalized (ANDERS & GREVESSE, 1989) REE patterns of samples Ž-1, Ž-2, Ž-3, Ž-4, Ž-7, Ž-10, Ž-11, Ž-16, Ž-17, Ž-19 and Ž-20 with Ž-Comp (= Ž-Composite).

composition of the upper continental crust (Fig. 11). Strontium is elevated in all samples, especially in samples Ž-3 (1862.5 ppm), Ž-1 (>1 mass. %), Ž-20 (928.5 ppm) and Ž-7 (>1 mass. %). Yttrium is slightly elevated in Ž-3 (24.8 ppm), Ž-11 (41 ppm) and Ž-19 (37.5 ppm) samples. Elevated concentrations of Ba and Sr have strong positive correlations with the amount of barite in the samples. An increased concentration of Y could be linked with the occurrence of fluorite in the samples.

Rare-earth element concentrations are presented in Appendix A. The ΣREE varies from 5.73 to 166.01 ppm in the analysed samples. In addition, visible enrichment of light REEs is present in most of the samples with the ΣLREE/ΣHREE ratio being highly fractionated where ΣLREE increases to 598.13 ppm and ΣHREE up to 24.42 ppm. They are normalized to chondrite (ANDERS & GREVESSE, 1989) (Fig. 12), where the higher concentration of LREEs is detected, with strong positive europium (Eu) and samarium (Sm) anomalies. Samples Ž-7, Ž-16 and Ž-20 have the most deviating positive Eu anomaly, with Eu/Eu* ratio 24.27; 20.28 and 20.89 respectively, and with a noticeable positive Sm anomaly. In these three samples, the concentration of Eu ranges from 40.73 to 43.52 ppm while Sm varies from 110.12 to 118.28 ppm. The Eu anomaly was calculated as $Eu/Eu^* = EuN/\sqrt{[(SmN)*(GdN)]}$. Other significant anomalies that are visible on diagrams include negative cerium (Ce) and ytterbium (Yb) anomalies. Trace and REEs normalized to Upper Continental Crust (TAYLOR & MCLENNAN, 1995) show similar trends in most of the samples, while samples Ž-1 and Ž-4 show no distinctive anomalies or deviating trends, just slightly increased, but equal, concentrations of all REEs.

To determine the correlation between the geochemical contents of major elements and trace elements, hierarchical cluster analysis (HCA) was conducted. The main principle in classification of the samples and variables in HCA is the visual observation of the constructed dendrogram. The HCA resulted in one dendrogram of analysed Ba-F vein mineralization samples (Fig. 14). Three geochemically different clusters can be distinguished. One cluster consists of BaO, SO_3 and SrO, grouped with Sm and Eu. Second cluster consists of CaO, F, NaO and majority of HREEs, while the third cluster consists of the remaining major elements (SiO_2, MgO, Fe_2O_3, etc.) with Nb and LREEs (Ce, Nd and Pr).

5. DISCUSSION

5.1. Structural control of the mineralization

Besides structural analysis, rupture zones through which hydrothermal fluids were circulating have been recognized as one of the main control factors of barite-fluorite ore mineralization. They filled out fault zones and veinlet systems with the breccia structure of the host rock, dolostone, making circulation easier. Fault orientation and position, when compared to a general dip of the beds (vertical to the strike), indicates pre-ore emplacement ESE-WNW oriented bedding, perpendicular to the current Dinaride NW-SE direction. Similar bedding orientation with pole concentration that highlights Pi-girdle with β-axis 14/15 was determined by GRUBIĆ & PROTIĆ (2003) while working on flysch sediments of the olistostromatic unit in the Adamuša deposit (situated 4 km west of the Žune deposit).

Five vein/veinlet systems were determined during fieldwork. Longitudinal veinlets made a strong contribution to other veinlets and in the destruction of the deposit near the surface, when in combination with other exogenous factors. Based on statistical data interpretation (Figs. 13A and 13B) of veinlets spatial positions that are filled with barite and fluorite, it was recognized that these veinlets occur in the aforementioned five veinlet systems. The main ESE-WNW vergency fault zone and Sv_2 barite and fluorite veinlets were formed during the Variscan orogeny. This is consistent with the observations of PALINKAŠ et al. (2016), interpreting Žune Ba-F mineralization as a shallow epithermal manifestation of the Late Permian Ljubija Fe polysulfide ore field. However, it must be taken into consideration that their morphological and genetic significance is not the same. Based on the remaining ore body material, it can be concluded that they were thicker and more significant than the remaining ruptures. This interpretation fits with the regional analysis of the Sana-Una Palaeozoic structures and rupture systems in the Adamuša iron de-

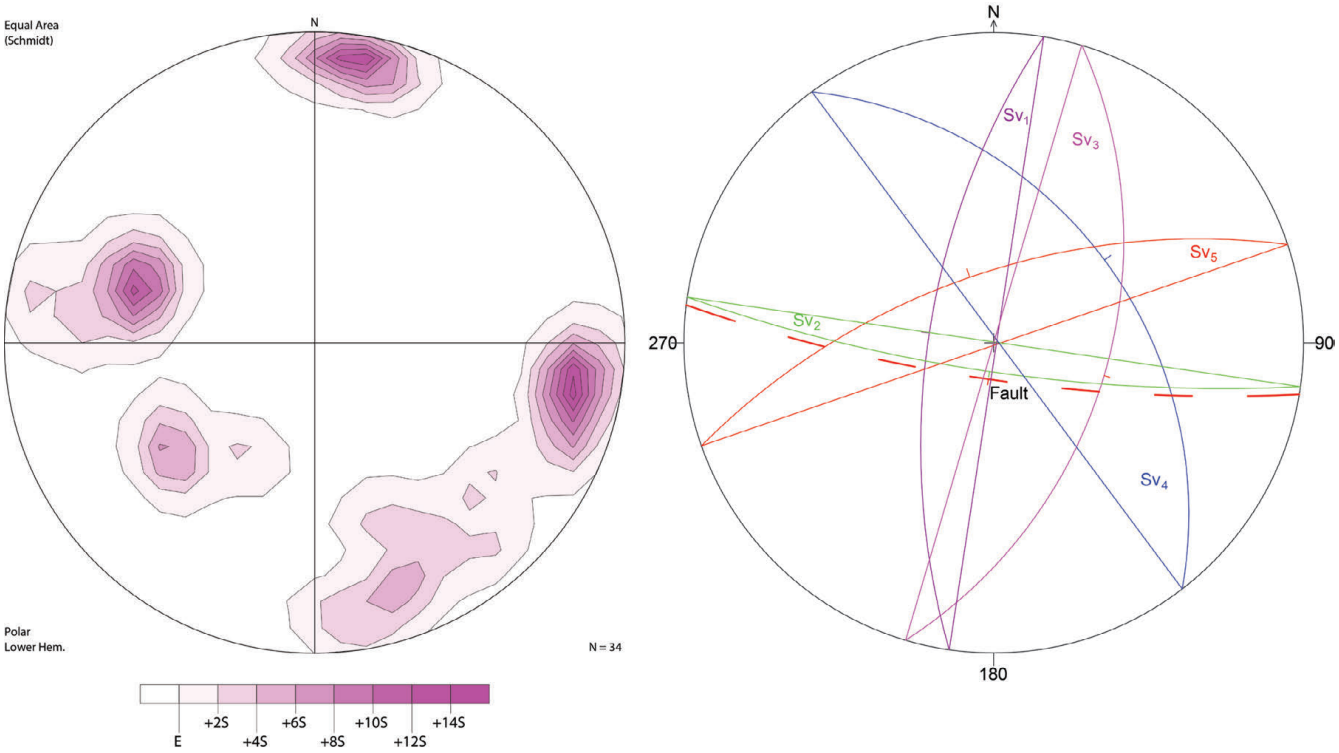

Figure 13. A) A contour diagram of poles to veins/veinlets in the quarry, determined through measurements of structural geology, n= 34; B) Stereographic projection (Schmidt net) for the vein/veinlet systems in the study area.

posit (GRUBIĆ et al., 2003). Many of these folded structures, in all dimensions, west of the Sana River and particularly between Ovanjska and Ravska have a β-axis positioned in a N-E to NNE-SSW direction (GRUBIĆ et al., 2015).

5.2. Ore deposition conditions

5.2.1. Contact zone

The mineralogical assemblage of the contact zone between the dolostone and vein-type mineralization is characterized by tremolite, magnesiochloritoid, topaz (pyknite) and epidote.

Tremolite [$Ca_2Mg_5Si_8O_{22}(OH)_2$] occurs in several samples (Ž-4, Ž-5, Ž-17 and Ž-19) in the Žune deposit. It is commonly developed on the fluorite-quartz-carbonate boundary so the presence of quartz indicates that the tremolite-forming reaction was not fully completed. The mineral assemblages suggest the reaction (SLAUGHTER et al., 1975; EGGERT & KERRICK, 1981):

$$\underset{\text{(dolomite)}}{5CaMg(CO_3)_2} + \underset{\text{(quartz)}}{8SiO_2} + H_2O = \underset{\text{(tremolite)}}{Ca_2Mg_5Si_8O_{22}(OH)_2} + \underset{\text{(calcite)}}{3CaCO_3} + 7CO_2. \quad (1)$$

Corresponding equilibrium conditions for reaction (1) were: a pressure of 2 kbars with a temperature of 484 +/- 15°C and X_{CO2}= 0.85. These data were the starting points for the thermodynamic calculation of phase equilibria in the CaO-MgO-SiO_2-H_2O-CO_2 system (SLAUGHTER et al., 1975). Reactions involving talc can be excluded as no talc was discovered in the carbonates of the Žune deposit area. The rare Tr + Dol assemblage reflects either local mineralogical (and hence compositional) zoning on a larger scale than a thin section, or local metasomatism (COOK & BOWMAN, 2000). BUCHER & FREY (2002) stated that in a zone with tremolite-bearing dolomites, the low temperature limit for tremolite coincides with the upper limit for talc (≈ 450°C).

Chloritoid [$(Fe^{2+},Mg,Mn^{2+})Al_2(SiO_4)O(OH)_2$] with *Magnesiochloritoid* [$MgAl_2(SiO_4)O(OH)_2$] as an Mg analogue is often a so-called "stress" mineral but it is also observed in quartz-carbonate veins and other hydrothermal environments according to DEER et al. (1997). Mg-chloritoid occurs in three samples (Ž-5, Ž-17 and Ž-19) where it occurs included in quartz. GHENT et al. (1989) suggested a Mg-chloritoid forming reaction as:

$$\underset{\text{(chlorite)}}{(Mg,Fe^{2+})_5Al(Si_3Al)O_{10}(OH)_8} + \underset{\text{(calcite)}}{4CaCO_3} + 4CO_2 = \underset{\text{(dolomite)}}{4CaMg(CO_3)_2} + \underset{\text{(quartz)}}{2SiO_2} + \underset{\text{(Mg-chloritoid)}}{MgAl_2(SiO_4)O(OH)_2}. \quad (2)$$

In reaction (2) GHENT et al. (1989) decided on a clinochlore component of chlorite that reacts with calcite giving Mg-chloritoid alongside recrystallised dolomite and quartz. The suggested conditions of formation were a constant total pressure of 5 kbars for part of the system K_2O-Na_2O-FeO-MgO-CaO-Al_2O_3-SiO_2-H_2O-CO_2, and X_{CO2} exceeding ≈ 0.01 at 350°C. LIVI et al. (2002) showed, in a series of mineral forming reactions, that the mineral assemblage Cal + Dol + Chl is present at a pressure of 2 kbars and a temperature range of 320-400°C. Although chlorite was not detected, due to the small number of thin-sections available, its presence cannot be ruled out, similar to GHENT et al. (1989) where chlorite was also lacking in the mineral assemblage.

Pyknite [$Al_2(SiO_4)(F,OH)_2$] is a variety of fine-grained topaz, but also commonly occurs as dense aggregates of prismatic to acanthine crystals. Pyknite occurs in three samples (Ž-5, Ž-17 and Ž-19) where it is found as inclusions in quartz grains. At low Ca^{2+}/H^+ activity ratios, topaz is a stable phase whereas fluorite is deposited at high Ca^{2+}/H^+ ion activity ratios (as referenced in

SRIVASTAVA & SUKHCHAIN, 2005). Under conditions of very high F-activity, topaz may form as a result of the instability of muscovite in the presence of HF according to the reaction (WRIGHT & KWAK, 1989):

$$\underset{\text{(muscovite)}}{K_2Al_2(Si_6Al_2O_{20})(OH)_4} + 3HF + 2H^+ =$$

$$\underset{\text{(topaz)}}{3Al_2(SiO_4)(OH,F)_2} + \underset{\text{(quartz)}}{3SiO_2} + 2K^+ + 4H_2O. \quad (3)$$

According to THOMAS (1994), who studied different types of topaz in the Erzgebirge area in Germany, temperatures of formation of hydrothermal topaz are ≤ 330°C with a fluorine content (in F/(F + OH) molar ration) of ≤ 0.76.

Epidote [$Ca_2(Al_2Fe^{3+})(Si_2O_7)(SiO_4)O(OH)$] occurs in four samples (Ž-2, Ž-9, Ž-15 and Ž-17) mostly present in granular aggregates. BIRD & SPIELER (2004) described the formation of epidote by precipitation in veins and cavities and by replacements of silicates, carbonates and Fe-oxides. Due to the sensitivity of epidote solid solutions to slight changes in fluid chemistry, the quantitative evaluation of the physical and chemical variables may be unreliable as stated in ARNASON et al. (1993). Thus, it must be taken into consideration that under hydrothermal conditions, epidote is stable over a range of temperatures and pressures (as referenced in BIRD & SPIELER, 2004).

5.2.2. Ba-F vein type mineralization (previous estimation)

The formation conditions of the *Žune Ba-F epithermal deposit as a part of* the Ljubija ore field were described by PALINKAŠ et al. (2016). These authors conducted various analyses: (i) microthermometric measurements; (ii) Laser Raman spectroscopy that was performed on fluorite samples and (iii) bulk crush-leach analysis by ionic chromatography that was performed on fluorite and barite samples from the Žune deposit. Fluid inclusion studies in fluorite from the fluorite-barite veins resulted in the discovery of nine different types of inclusions. Liquid-rich and vapour-rich inclusions with or without daughter minerals were the objects of the study. Homogenization temperatures were in a range from 125°C to 245°C for liquid-rich inclusions of high salinity, and vapour-rich inclusions with very low salinity. Laser Raman spectroscopy was also performed on liquid-rich aqueous inclusions containing halite daughter minerals, with high salinity. The inclusions were composed of aqueous liquid and aqueous gas and/or traces of CO_2 at room temperature, while other volatiles were not detected. Maximum values of SO_4^{2-} were up to 30.000 ppm within a single fluorite sample which is explained by contamination with barite since it was very often found in paragenesis. Hydrothermal fluids were represented as a mixture of high-temperature-high salinity Permian evaporitic sea water, diluted by low-temperature-low-salinity sea or meteoric waters (PALINKAŠ et al., 2016). The boiling temperature was controlled by the hydrostatic pressure at depths of 100-200 m below the land surface so the Žune ore deposit experienced intensive boiling due to the near-surface setting.

5.3. Hierarchical cluster analysis of geochemical data

Establishing the relationship between major-, trace- and REEs was based on two main approaches: plotting trace and REEs and a hierarchical cluster analysis (HCA).

5.3.1. The role of barite

The highest Sr concentrations occur in the samples containing the highest amount of barite (e.g. Ž-7, Ž-19 and Ž-20 sample; Appendix A). The presence of Sr in the barite can be explained by the substitution of Ba^{2+} with Sr^{2+} in the crystal lattice due to similar ionic radii (Ba= 1.42 Å; Sr= 1.26 Å) and expressed as a $SrSO_4$ component. Such a relatively high Sr content is typical for an ascending hydrothermal type of mineralization, whereas a low content characterizes the volcano-sedimentary type of barite deposit (JURKOVIĆ et al., 2010). Additionally, JURKOVIĆ et al. (2010) presented the relationship between the $SrSO_4$ content in barites of Bosnia and other worldwide known barite deposits. They determined that the barite of Bosnia, those of the Brixlegg deposit in Austria and the Rudnany deposit in Slovakia are characterized by considerably higher $SrSO_4$ contents which is typical for hydro-

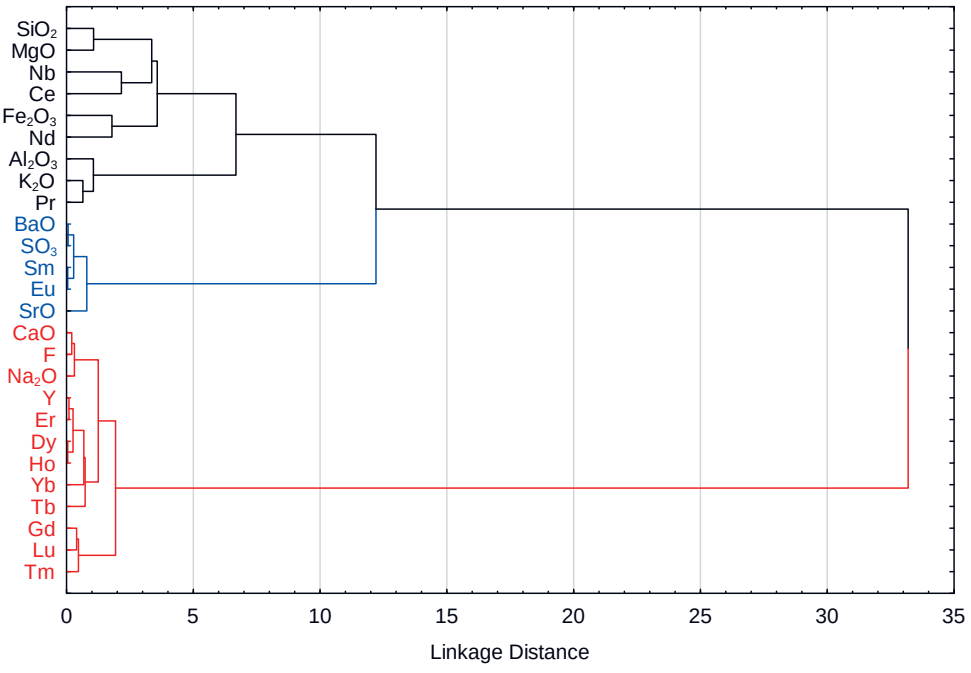

Figure 14. Hierarchical cluster analysis of the Ba-F vein mineralization and hydrothermal breccia samples.

thermal epigenetic deposits. The conclusion was that the extended ranges of $SrSO_4$ contents could be the result of partial remobilization processes during the Variscan and Alpine orogenies.

The most significant difference in the REE distribution patterns is observed in the Sm- and Eu-anomaly that is mildly positive for most of the samples (Fig. 12), but highest in the Ž-7, Ž-16 and Ž-20 samples (Appendix A). Higher concentrations of Sm and Eu also follow the trend of the higher amount of barite in the samples which suggests that there is an enrichment of those two LREEs in barite. A negative correlation between Sm and Eu with CaO, MgO and F (Appendix B) is noted, meaning that there is no Sm and Eu enrichment in either the dolomite or fluorite phases. This result suggests that the ore-forming hydrothermal fluid was enriched in Sm and Eu, which were presumably incorporated into the barite. HAJALILOU et al. (2014) stated that the positive Eu anomaly can be caused due to reducing conditions that stabilize Eu^{2+}. They added that if the ore-forming fluid is the final stage of the magmatic differentiation, the late fluid is enriched in Eu, K, Ba and Sr, where Eu^{2+} and Sr^{2+} are similar to Ba^{2+}, leading to their involvement in the barite structure. BAU & MÖLLER (1992) (as referenced in SAFINA et al., 2021) suggested that a positive Eu anomaly could indicate a high temperature of mineral formation (>250°C), with reducing conditions and the presence of Eu^{2+} in the mineralizing fluid. MORGAN et al. (1980) deemed it is more likely that the positive Eu anomaly is related to the large radius of the Eu^{2+} cations. The bigger the REE ions, the more easily they'll be incorporated into the barite structure due to the large Ba^{2+} ionic radius (1.50 Å stated by MORGAN et al., 1980, but 1.42 Å by renewed data). The Eu^{2+} ion is very similar in size and charge to Sr^{2+} (1.33 Å in VIII co-ordination) and accordingly is less difficult to accommodate in the barite structure than the smaller trivalent REEs; in addition, Eu^{2+} requires no charge compensation (MORGAN et al., 1980). Based on renewed data, the ionic radius of Eu^{2+} is 1.25 and Sr^{2+} is 1.26 in VIII co-ordination. So, it can be concluded that minerals with large ions, such as Ba^{2+} (1.42 Å), favour replacement by the largest (=lightest) REE ions (MORGAN et al., 1980), such as Eu and the neighbouring Sm. When compared to hierarchical cluster analysis (Fig. 14) Sm and Eu make one cluster that is connected to BaO and SO_3, which proves their strong connection. SrO makes contact with BaO-SO_3-Eu-Sm cluster somewhat later, implying a secondary connection to it. This could indicate that barite was first enriched in REEs (Sm and Eu) and then later with Sr.

5.3.2. The role of fluorite

Most of the samples containing a higher amount of the fluorite phase also show higher concentrations of yttrium and other HREEs (e.g. Ž-3, Ž-11 and Ž-19 samples). While barite can also be found in these samples, there is a negative correlation between Y and barite (Appendix B) and in contrast, a positive correlation between Y and fluorite.

Typically, fluorite is associated with several critical elements, including REE, Y and Nb. Yttrium is considered to be a pseudo-lanthanide due to its similar size and the same charge as the lanthanides, and it behaves anomalously in F-rich systems (as referenced in MAGYAROSI & CONLIFFE, 2021). These authors also stated that the positive Y anomaly is a common feature of hydrothermal fluorites. As observed in Fig. 11, Y shows a slightly positive anomaly in Ž-3, Ž-11 and Ž-19 samples. This could be explained by yttrium forming a complex with fluorine due to the substitution of Ca^{2+} (ionic radius of 1.00 Å) and Y^{3+} (ionic radius of 1.02 Å). In addition, MÖLLER et al. (1998) suggested that to achieve electrical neutrality due to substitutions of ions of different charges, the following types of reactions should be considered:

1. $2Ca^{2+} \leftrightarrow REE^{3+} + Na^{+}$;
2. $3Ca^{2+} \leftrightarrow 2\ REE^{3+} + \square$;
3. $Ca^{2+} \leftrightarrow REE^{3+} + F^{-}$.

So the previously mentioned substitution would be possible according to reaction (3) where instead of REE^{3+} in the reaction there would be Y^{3+}. There is also a positive correlation between HREEs and Na_2O with fluorite (Appendix B) meaning fluorite is slightly enriched with HREE and depleted in LREE. According to MÖLLER et al. (1998) partial dissolution due to tectonic stress and subsequent recrystallisation leads to the preferred separation of LREE from fluorite. Also, LREE are dominantly present in a separate phase, which has a different solubility behaviour than fluorite and therefore, due to remobilization, the subsequently precipitated fluorite is considerably depleted in LREE. Moreover, LREE fractionation also occurs during precipitation of fluorite due to HREE forming more stable fluoro-complexes and staying in the F-rich fluid. With Na (Na_2O in Appendix B) showing a positive correlation with HREE and fluorite, a possible explanation would be that Na^{+} forms complexes with REE^{3+} while substituting Ca^{2+} according to the previously mentioned reaction (1). MÖLLER et al. (1998) (as referenced in MAGYAROSI & CONLIFFE, 2021) noted that the positive correlation of Na with the total REE-Y content observed in some phases suggests that the Ca^{2+} atom in the structure of fluorite is replaced by REE-Y^{3+}, with Na^{+} preserving an electrically neutral charge in these phases.

6. CONCLUSION

This manuscript is focused on the Žune Ba-F epithermal deposit, situated in the Ljubija ore field of northwestern Bosnia and Herzegovina, bringing new data on field mapping, the structural setting, mineralogy and geochemistry. Different lithological units were determined and analysed: Upper Palaeozoic dolostone is the host rock, contact zone, Ba-F vein type and hydrothermal breccia mineralization. The dolostone is characterized by external and internal pseudo-bedding (steepening to 50-55° dip towards the east) with a massive, homogeneous structure, dark grey in colour, with signs of partial limonitization proximal to mineralization and composed of dolomite mineral grains with negligible amounts of muscovite and opaque pyrite.

The contact zone consists of hydrothermally recrystallized host dolostone with early quartz and pyrite, whereas the presence of accessory minerals including tremolite, magnesiochloritoid and pyknite indicate higher temperatures of formation, generally above 300°C. The data obtained represent local peak temperature conditions in the contact zone related to the pre-mineralization stage and correspond to previously reported peak microthermometric temperatures on coarse-grained fluorite from the main mineralization stage. XRD analysis of the light mineral fraction confirmed dolomite, calcite and fluorite with minor quartz and occasional chloritoid.

Structural analysis of the Ba-F mineralization recognized five vein/veinlet systems, infilled with barite and fluorite. The most important system (Sv_2) stretches vertically to subvertically to the pseudo-bedding with an orientation of 190/80, and was formed during the Variscan orogeny. Fluorite and quartz are usually located on the veinlet's edges indicating slightly earlier deposition, while barite is dominant in the central part of the veins, indicating somewhat later deposition. Hydrothermal breccia is composed of

coarse-grained barite and fluorite surrounding irregular fragments of dolostone, crosscut by quartz-limonite veinlets, pointing to hydraulic fracturing, with the breccia occupying ≈20 % of the deposit.

Geochemical analysis revealed elevated BaO, SO_3, CaO and F contents in the mineralized zone, while CaO and MgO were elevated in the dolostone. Barite-rich samples have elevated Sr contents that are typical for barite-rich epigenetic hydrothermal ore deposits in the Dinarides, due to Ba-Sr substitutions in the barite crystal lattice. Fluorite-rich samples are characterized by enrichment in Y (0.6 – 49.2 ppm) and HREEs accompanied by depletion of LREEs. Hierarchical cluster analysis confirmed the correlation between the barite phase with SrO and LREEs (Sm and Eu), indicating that the barite-forming hydrothermal fluid was possibly enriched with Sm and Eu. CaO and Na_2O are clustered together with F, Y and other REEs that refer to the formation of fluorite and substitution reactions between Ca, Na, F, Y and other HREEs. Due to having variable REE concentration and low to moderate negative cerium and ytterbium anomalies, the Ba-F Žune deposit corresponds to the fluorite deposits associated with carbonate sedimentary rocks according to the classification scheme.

ACKNOWLEDGEMENT

This work has been financially supported by EIT RawMaterials project no. 17051 Invest RM: Multifactor model for investments in the raw material sector, a part of the Horizon 2020 program. We would like to thank the Invest RM team (https://investrm.eu/) for continuous fieldwork support, helpful advice and discussion, especially colleagues from the Mining Institute Prijedor supervised by director Dragoja LAJIĆ with scientific support of prof. Ranko CVIJIĆ.

REFERENCES

ANDERS, E. & GREVESSE, N. (1989): Abundances of the elements: meteoric and solar.– Geochim. Cosmochim. Ac., 53/1, 197–214. doi: 10.1016/0016-7037(89)90286-X

ARNASON, J.G., BIRD, D.K. & LIOU, J.G. (1993): Variables Controlling Epidote Composition in Hydrothermal and Low-Pressure Regional Metamorphic Rocks.– Abh. Geol. Bundesanst. Wien, 49, 17–25.

BAU, M. & MÖLLER, P. (1992): Rare earth element fractionation in metamorphogenic hydrothermal calcite, magnesite and siderite.– Miner. Petrol., 45/3-4, 231–246. doi: 10.1007/bf01163114

BAU, M. & DULSKI, P. (1995): Comparative study of yttrium and rare-earth Element behaviours in fluorine rich hydrothermal fluids.– Contrib. Mineral. Petr., 119/2–3, 213–223. doi: 10.1007/BF00307282

BEJAOUI, J., BOUHLEL, S. & BARCA, D. (2013): Geology, Mineralogy and Fluid Inclusions Investigation of the Fluorite Deposit at Jebel Kohol, northeastern Tunisia.– Period. Mineral., 82/2, 217–237. doi: 10.2451/2013PM0013

BIRD, D.K. & SPIELER, A.R. (2004): Epidote in Geothermal Systems.– Rev. Mineral. Geochem., 56/1, 235–300. doi: 10.2138/gsrmg.56.1.235

BOROJEVIĆ ŠOŠTARI, S., GIANNAKOPOULOU, S., ADAM, K. & MILEUSNIĆ, M. (2022): The future of mining in the Adria region: current status, SWOT and Gap analysis of the mineral sector.– Geol. Croat., 75/3, 317–334. doi: 10.4154/gc.2022.26

BUCHER, K. & FREY, M. (2002): Petrogenesis of Metamorphic Rocks.– Springer-Verlag, Berlin, 341 p. doi: 10.1007/978-3-662-04914-3

COOK, S.J. & BOWMAN, J.R. (2000): Mineralogical Evidence for Fluid–Rock Interaction Accompanying Prograde Contact Metamorphism of Siliceous Dolomites: Alta Stock Aureole, Utah, USA.– J. Petrol., 41/6, 739–757. doi: 10.1093/petrology/41.6.739

DEER, W.A., HOWIE, R.A. & ZUSSMAN, J. (1997): Rock-forming minerals.– The Geological Society of London, London, 936 p.

EGGERT, R.G. & KERRICK, D.M. (1981): Metamorphic equilibria in the siliceous dolomite system: 6 kbar experimental data and geologic implications.– Geochim. Cosmochim. Ac., 45/7, 1039–1049. doi: 10.1016/0016-7037(81)90130-7

GHENT, E.D, STOUT, M.Z. & FERRI, F. (1989): Chloritoid-paragonite-phyrophyllite and stilpnomelane bearing rocks near Blackwater Mountain, western Rocky Mountains, British Columbia.– Can. Mineral., 27/1, 59–66.

GRUBIĆ A., PROTIĆ, L.J., FILIPOVIĆ, I. & JOVANOVIĆ, D. (2000): New data on the Palaeozoic of the Sana-Una Area.– In: Proceedings of the International Symposium of the Dinarides and the Vardar Zone. Acad. Sci. Art. Rep. Serb., Dept. Natur. Math. and Tech. Sci. I., Banja Luka, 49–54.

GRUBIĆ, A. & PROTIĆ, LJ. (2003): Studija strukturnih i genetskih karakteristika Tomašičkog rudnog polja [*The study of structural and genetical characteristics of Tomašica ore field* – in Serbian].– In: GRUBIĆ, A. & CVIJIĆ, R. (eds.): Novi prilozi za geologiju i metalogeniju rudnika gvožđa "Ljubija" [*New Contribution to the Geology and Metallogeny of the Ljubija Iron Ore Mine* – in Serbian]. Institute of Mining Prijedor and Mines of Iron ore "Ljubija" Prijedor, Prijedor, 63–134.

GRUBIĆ, A., CVIJIĆ, R., MILOŠEVIĆ, A. & ČELEBIĆ, M. (2015): Importance of olistostrome member for metallogeny of Ljubija iron ore deposits.– Archives for Technical Sciences, 13/1, 1–8. doi: 10.7251/afts.2015.0713.001G

HAJALILOU, B., VUSUQ, B. & MOAYED, M. (2014): REE Geochemistry of Precambrian Shale-Hosted Barite-Galena Mineralization, a Case Study from NW Iran.– Iranian Journal of Crystallography and Mineralogy, 22/2, 39–48.

JANOUŠEK, V., FARROW, C.M. & ERBAN, V. (2006): Interpretation of whole-rock geochemical data in igneous geochemistry: introducing Geochemical Data Toolkit (GCDkit).– J. Petrol., 47/6, 1255–1259. doi:10.1093/petrology/egl013

JEREMIĆ, M. (1958): Baritno-fluoritno ležište Žune kod Ljubije [*Barite-flourite deposit Žune-Dolinac near Ljubija* – in Serbian].– Rudarsko-metalurški zbornik, 4, Ljubljana.

JURIĆ, M. (1971): Geologija područja Sanskog paleozoika u sjeverozapadnoj Bosni [*Geology of the Sana Palaeozoic area in NW Bosnia* – in Croatian].– Geološki glasnik XI, Sarajevo, 146 p.

JURKOVIĆ, I., GARAŠIĆ, V. & HRVATOVIĆ, H. (2010): Geochemical characteristics of barite occurrences in the Palaeozoic complex of South-eastern Bosnia and their relationship to the barite deposits of the Mid-Bosnian Schist Mountains.– Geol. Croat., 63/2, 241–258. doi: 104154/gc.2010.20

KARAMATA S., KRSTIĆ B., DIMITRIJEVIĆ M.D., DIMITRIJEVIĆ M.N., KNEŽEVIĆ V., STOJANOV, R. & FILIPOVIĆ, I. (1997): Terranes between the Moesian Plate and the Adriatic Sea.– Ann. Geol. Pays Hellén., 37/1, 429–477.

LIVI, K.J.T., FERRY, J.M., VEBLEN, D.R., FREY, M. & CONNOLLY, J.A.D. (2002): Reactions and physical conditions during metamorphism of Liassic aluminous black shales and marls in central Switzerland.– Eur. J. Mineral., 14/4, 647–672. doi: 10.1127/0935-1221/2002/0014-0647

MAGOTRA, R., NAMGA, S., ARORA, N. & SRIVASTAVA, P.K. (2017): New Classification Scheme of Fluorite Deposits.– International Journal of Geosciences, 8/4, 599–610. doi: 10.4236/ijg.2017.84032

MAGYAROSI, Z. & CONLIFFE, J. (2021): REE-Y patterns and fluid inclusion analysis of fluorites from the AGS fluorite deposit, St. Lawrence, Newfoundland.– Newfoundland and Labrador Department of Industry, Energy and Technology Geological Survey, Report 21–1, 27–47.

MAJER, V. (1964): Petrografija paleozojskih sedimenata sjeveroistočnog dijela Trgovske gore [*Petrography of Palaeozoic sediments from the North-Eastern parts of the Trgovska Gora Mt* – in Croatian with an English abstract].– Geološki vjesnik, 17, 79–92.

MILOŠEVIĆ, A., GRUBIĆ, A., CVIJIĆ, R. & ČELEBIĆ, M. (2017): Annexes the knowledge of the metalogenia of the Ljubija mineral area.– In: Book of Proceedings, 7th Balkan mine congress. Prijedor, 57–68.

MÖLLER, P., BAU, M., DULSKI, P. & LÜDERS, V. (1998): REE and yttrium fractionation in fluorite and their bearing on fluorite formation.– In: HAGNI, R.D. (ed.): Proceedings of the Ninth Quadrennial IAGOD Symposium. International Association on the Genesis of Ore Deposits, IAGOD, 575–592.

MORGAN, J.W. & WANDLESS, G.A. (1980): Rare earth element distribution in some hydrothermal minerals: evidence for crystallographic control.– Geochim. Cosmochim. Acta, 44/7, 973–980. doi: 10.1016/0016-7037(80)90286-0

PALINKAŠ, A.L., BOROJEVIĆ ŠOŠTARIĆ, S., STRMIĆ PALINKAŠ, S., PROCHASKA, W., PÉCSKAY, Z., NEUBAUER, F. & SPANGENBERG, J.E. (2016): The Ljubija geothermal field: A herald of the Pangea break-up (NW Bosnia and Herzegovina).– Geol. Croat., 69/1, 3–30. doi: 10.4154/gc.2016.02

PAMIĆ, J. (1993): Eoalpine to Neoalpine magmatic and metamorphic processes in the northwestern Vardar Zone, the easternmost Periadriatic Zone and the southwestern Pannonian Basin.– Tectonophysics, 226/1–4, 503–518. doi: 10.1016/0040-1951(93)90135-7

PAMIĆ, J., AMIĆ, J., GUŠIĆ, I. & JELASKA, V. (1998): Geodynamic evolution of the central Dinarides.– Tectonophysics, 297/1–4, 251–268. doi: 10.1016/S0040-1951(98)00171-1

PAMIĆ, J. & JURKOVIĆ, I. (2002): Palaeozoic tectonostratigraphic units of the northwest and central Dinarides and the adjoining South Tisia.– Int. J. Earth. Sci., 91, 538–554. doi: 10.1007/s00531-001-0229-8

RAJABZADEH, M.A. (2007): A fluid inclusion study of a large MVT barite-fluorite deposit: Komshecheh, Central Iran.– Iran. J. Sci. Technol. A., 31/A1, 73–87.

SAFINA, N.P., SOROKA, E.I., ANKUSHEVA, N.N., KISELEVA, D.V., BLINOV, I.A. & SADYKOV, S.A. (2021): Fluorite in Ores of the Saf'yanovka Massive Sulfide Deposit, Central Urals: Assemblages, Composition, and Genesis.– Geol. Ore Deposits, 63/2, 118–137. doi: 10.1134/S1075701521020057

SCHMID, S.M., BERZA, T., DIACONESCU, V., FROITZHEIM, N. & FÜGENSCHUH, B. (1998): Orogen-parallel extension in the Southern Carpathians.– Tectonophysics, 297/1, 209–228. doi: 10.1016/S0040-1951(98)00169-3

SLAUGHTER, J., KERRICK, D.M. & WALL, V.J. (1975): Experimental and thermodynamic study of equilibria in the system CaO–MgO–SiO_2–H_2O–CO_2.– Am. J. Sci., 275/2, 143–162. doi: 10.2475/ajs.275.2.14

SRIVASTAVA, P.K. & SUKCHAIN (2005): Petrographic Characteristics and Alteration Geochemistry Granite-hosted Tungsten Mineralization at Degana, NW India.– Resour. Geol., 55/4, 373–384. doi: 10.1111/j.1751-3928.2005.tb00258.x

STATSOFT, INC. (2012): Electronic Statistics Textbook. Tulsa, OK: StatSoft. Available form: <http://www.statsoft.com/textbook/>.

TAYLOR, S.R. & MCLENNAN, S.M. (1995): The geochemical evolution of the continental crust.– Rev. Geophys., 33/1, 241–265. doi: 10.1029/95RG00262

THOMAS, R. (1994): Fluid evolution in relation to the emplacement of the Variscan granites in the Erzgebirge region: A review of the melt and fluid inclusion evidence.– In: SELTMANN, R., KÄMPF, H. & MÖLLER P. (eds): Metallogeny of Collisional Orogens. Czech Geological Survey, Prague, 70–81.

TOMLJENOVIĆ, B. (2002): Strukturne značajke Medvednice i Samoborskog gorja [*Structural characteristics of the Mt. Medvednica and the Samoborsko gorje Mt.* – in Croatian].– PhD Thesis, Faculty of Mining, Geology and Petroleum engineering, University of Zagreb, 208 p.

WILLINGSHOFER, E. (2000): Extensionin collisional orogenic belts: the Late Cretaceous evolution of the Alps and Carpathians.– PhD Thesis, Vrije University, Amsterdam, 146 p.

WRIGHT, J.H. & KWAK, T.A.P. (1989): Tin-bearing greisens of Mount Bischoff, northwestern Tasmania, Australia.– Econ. Geol., 84/3, 551–574. doi: 10.2113/gsecongeo.84.3.551

XU, C., TAYLOR, R.N., LI, W., KYNICKY, J., CHAKHMOURADIAN, A.R. & SONG, W. (2012): Comparison of fluorite geochemistry from REE deposits in the Panxi region and Bayan Obo.– China. J. Asian. Earth. Sci., 57, 76–89. doi: 10.1016/j.jseaes.2012.06.007

Appendix A

Sample type	Dolostone					Ba-F vein type mineralization					Hydrothermal breccia	
Sample	Ž-1	Ž-2	Ž-4	Ž-10	Ž-17	Ž-3	Ž-11	Ž-16	Ž-19	Ž-20	Ž-7	**Ž-Comp**
SiO_2	2.20	2.06	1.33	1.74	3.65	5.77	2.92	3.28	4.29	3.90	5.53	5.31
TiO_2	0.03	0.02	0.02	0.01	0.02	<0.01	<0.01	<0.01	<0.01	<0.01	0.01	0.01
Al_2O_3	0.74	0.37	0.38	0.27	0.32	0.35	0.38	0.09	0.30	0.16	0.24	0.32
Fe_2O_3	0.85	0.75	0.78	0.87	0.75	0.30	0.07	0.09	0.04	0.15	0.17	0.81
Cr_2O_3	<0.01	<0.01	<0.01	<0.01	<0.01	<0.01	<0.01	<0.01	<0.01	<0.01	<0.01	<0.01
MgO	17.14	17.35	16.47	16.48	15.62	0.78	0.02	0.10	0.17	0.37	0.55	5.75
MnO	0.11	0.11	0.10	0.11	0.10	0.01	<0.01	<0.01	<0.01	<0.01	<0.01	0.06
CaO	31.96	32.38	31.15	30.24	30.81	49.06	65.10	7.98	66.03	6.30	1.71	28.61
K_2O	0.15	0.06	0.06	0.05	0.04	0.06	0.05	0.02	0.04	0.03	0.05	0.06
Na_2O	0.06	0.06	0.07	0.05	0.06	0.17	0.26	0.05	0.25	0.05	0.02	0.09
P_2O_5	0.02	<0.01	<0.01	<0.01	<0.01	<0.01	<0.01	<0.01	0.02	<0.01	<0.01	<0.01
BaO	0.28	0.83	0.02	0.51	0.39	15.93	5.68	49.05	3.92	50.23	50.74	23.35
SrO	<0.01	0.01	<0.01	0.01	<0.01	0.23	0.08	1.26	0.12	1.17	1.26	0.52
SO_3 *	0.15	0.43	0.01	0.27	0.20	8.32	2.97	25.61	2.05	26.22	26.49	12.19
F *	2.83	2.87	2.87	2.55	3.16	16.68	22.63	2.73	22.88	2.01	0.33	7.36 **
LOI	45.22	45.18	45.58	44.60	43.61	3.12	0.30	1.28	0.44	0.90	0.95	13.39
Total	101.73	102.49	98.84	97.75	98.74	100.78	100.45	91.53	100.54	91.50	88.05	97.83
Ba	2110	6126	184	4238	3107	1426	8391	1739	8044	2040	1889	953
Be	0.28	0.14	0.17	0.27	0.33	0.14	0.10	0.13	0.79	0.06	<0.05	0.35
Co	0.4	0.4	0.6	0.9	0.5	0.9	1.5	0.5	0.2	1.0	3.4	3.7
Cs	0.32	0.10	0.14	0.07	0.07	0.09	0.10	0.04	0.07	0.05	0.08	0.10
Ga	1.8	1.2	1.1	1.1	0.8	0.7	0.5	0.2	0.4	0.3	0.7	0.7
Hf	1.2	1.8	<0.2	<0.2	0.2	7.6	2.3	1.0	0.9	0.8	0.9	0.7
Nb	0.6	0.3	0.2	0.2	0.4	0.1	0.1	<0.10	<0.10	<0.10	0.2	0.2
Rb	6.1	2.6	2.6	1.9	1.7	2.7	2.3	1.2	2.5	1.8	2.4	1.9
Sn	0.3	<0.2	<0.2	<0.2	0.2	<0.2	<0.2	<0.2	<0.2	<0.2	0.5	0.3
Sr	64.8	111.2	61.7	120.4	99.6	1862.5	635.5	>10000	999.4	9248.5	>10000	4116.0
Ta	<0.1	<0.1	<0.1	<0.1	0.2	3.0	2.2	0.8	1.9	0.5	0.2	0.9
Sc	0.8	0.5	0.4	0.5	0.6	0.3	0.1	<0.1	<0.1	<0.1	0.1	0.4
Th	0.67	0.45	0.16	0.14	0.33	0.68	0.46	<0.05	0.30	<0.05	<0.05	0.09
U	0.39	0.53	0.94	0.61	0.30	0.22	0.17	<0.05	0.07	0.07	0.17	0.34
V	<10.00	<10.00	96	<10.00	20	122	56	<10.00	23	<10.00	<10.00	11
W	1	<1	2	2	1	4	2	2	2	2	1	2
Zr	6	17	<2	<2	<2	73	24	<2	12	<2	<2	<2
Y	7.1	2.9	3.9	3.7	3.6	24.8	41.6	5.9	37.5	5.5	3.5	16.8
Mo	0.10	0.13	0.07	0.09	0.09	0.09	<0.05	0.08	0.09	0.05	0.06	0.18
Cu	12.8	8.0	13.0	4.7	2.4	3.4	4.1	2.6	1.5	6.4	7.6	8.7
Pb	2.3	2.0	2.3	3.7	3.9	3.5	4.4	2.7	6.7	8.4	5.2	6.8
Zn	6	6	5	7	5	3	<2	<2	<2	<2	2	7
Ni	65.9	89.2	81.3	102.9	34.8	33.8	25.5	57.2	74.7	24.0	33.1	7.1
As	91.7	156.2	9.5	5.0	0.4	8.8	2.4	2.5	2.7	3.2	4.5	15.7
Cd	<0.02	0.03	<0.02	0.04	<0.02	0.02	0.02	0.03	<0.02	<0.02	0.02	0.05
Sb	7.4	2.4	1.6	2.5	2.1	0.9	0.8	0.8	<0.5	2.0	1.8	6.2
Bi	0.01	0.01	0.02	0.02	<0.01	0.01	0.01	0.01	<0.01	<0.01	0.08	0.02
Ag	0.11	0.06	0.05	0.03	0.02	0.02	0.02	0.02	0.02	0.03	0.06	0.08
Tl	0.29	0.22	0.05	0.03	<0.02	0.03	<0.02	<0.02	<0.02	<0.02	0.02	0.06
Se	<1.00	<1.00	<1.00	<1.00	<1.00	<1.00	<1.00	<1.00	<1.00	<1.00	<1.00	<1.00
La	3.5	1.7	0.9	1.6	1.7	0.5	0.5	0.5	0.5	0.5	0.5	0.9
Ce	7.12	3.45	1.87	3.02	3.34	0.49	0.40	0.09	0.26	0.47	0.96	1.49
Pr	0.79	0.38	0.26	0.33	0.36	0.21	0.22	0.03	0.08	0.07	0.15	0.60
Nd	3.5	1.6	1	1.2	1.6	1.5	1.3	1.7	0.7	1.7	2.1	1.6
Sm	1.12	2.02	0.32	1.63	1.42	31.14	11.36	110.12	8.88	112.27	118.28	44.93
Eu	0.31	0.64	0.08	0.57	0.48	10.87	4.24	40.59	3.29	40.33	43.52	16.23

Appendix A – continued.

Sample type	Dolostone					Ba-F vein type mineralization				Hydrothermal breccia	
Sample	Ž-1	Ž-2	Ž-4	Ž-10	Ž-17	Ž-3	Ž-11	Ž-16	Ž-19	Ž-20	Ž-7	**Ž-Comp**
Gd	0.63	0.26	0.34	0.31	0.36	0.80	1.55	0.34	1.71	0.31	0.25	0.72
Tb	0.10	0.05	0.06	0.05	0.07	0.19	0.38	0.09	0.30	0.10	0.06	0.17
Dy	0.67	0.29	0.34	0.30	0.42	1.09	2.28	0.18	1.86	0.12	0.06	0.83
Ho	0.14	0.06	0.07	0.07	0.08	0.21	0.42	0.03	0.36	0.02	0.01	0.16
Er	0.41	0.17	0.23	0.18	0.23	0.52	0.95	0.09	0.87	0.08	0.04	0.44
Tm	0.05	0.02	0.03	0.03	0.04	0.05	0.09	0.03	0.10	0.03	0.03	0.06
Yb	0.36	0.16	0.20	0.13	0.21	0.25	0.43	0.07	0.53	0.03	0.03	0.29
Lu	0.05	0.02	0.03	0.02	0.03	0.04	0.05	0.02	0.06	0.02	0.02	0.04
ΣREE	18.75	10.82	5.73	9.44	10.34	47.86	24.17	153.88	19.50	156.05	166.01	68.12
Eu/Eu*	1.13	2.71	0.73	2.45	2.05	6.66	3.09	20.28	2.58	20.89	24.47	8.73

* - stechiometrically calculated; ** - content determined in Czech Geological Survey laboratory

Appendix B

	BaO	CaO	MgO	MnO	Na_2O	SrO	Fluor	SO_3	Sm	Eu	Y
BaO	1										
CaO	-0.71	1									
MgO	-0.67	-0.03	1								
MnO	-0.67	-0.03	0.99	1							
Na_2O	-0.34	0.90	-0.45	-0.45	1						
SrO	0.99	-0.74	-0.64	-0.63	-0.38	1					
Fluor	-0.30	0.88	-0.50	-0.50	0.99	-0.34	1				
SO_3	1.00	-0.71	-0.68	-0.67	-0.34	0.99	-0.30	1			
Sm	0.99	-0.73	-0.66	-0.66	-0.36	0.99	-0.32	0.99	1		
Eu	0.99	-0.73	-0.66	-0.66	-0.36	0.99	-0.32	0.99	0.99	1	
Y	-0.21	0.83	-0.56	-0.55	0.98	-0.25	0.98	-0.21	-0.24	-0.24	1